Ultrasonics 62 (2015) 3–19

Contents lists available at ScienceDirect

Ultrasonics

journal homepage: www.elsevier.com/locate/ultras

Review of magnetostrictive patch transducers and applications in ultrasonic nondestructive testing of waveguides

Yoon Young Kim *, Young Eui Kwon [1]

School of Mechanical and Aerospace Engineering and Institute of Advanced Machines and Design, Seoul National University, 1 Gwanak-ro, Gwanak-gu, Seoul 151-742, Republic of Korea

ARTICLE INFO

Article history:
Received 9 January 2015
Received in revised form 4 May 2015
Accepted 19 May 2015
Available online 23 May 2015

Keywords:
Magnetostrictive patch transducer
Ultrasonic non-destructive testing
Waveguides

ABSTRACT

A magnetostrictive patch transducer (MPT) is a transducer that exploits the magnetostrictive phenomena representing interactions between mechanical and magnetic fields in ferromagnetic materials. Since MPT technology was mainly developed and applied for nondestructive ultrasonic testing in waveguides such as pipes and plates, this paper will accordingly review advances of this technology in such a context. An MPT consists of a magnetic circuit composed of permanent magnets and coils, and a thin magnetostrictive patch that works as a sensing and actuating element which is bonded onto or coupled with a test waveguide. The configurations of the circuit and magnetostrictive patch therefore critically affect the performance of an MPT as well as the excited and measured wave modes in a waveguide. In this paper, a variety of state-of-the-art MPT configurations and their applications will be reviewed along with the working principle of this transducer type. The use of MPTs in wave experiments involving phononic crystals and elastic metamaterials is also briefly introduced.

Contents

1. Introduction

Magnetostrictive transducers operate in accordance with the magnetostrictive principle. They have been used to generate and measure ultrasonic waves at frequencies ranging between roughly 20 kHz and 1–2 MHz for nondestructive testing (NDT) of waveguides such as pipes and plates. This paper reviews the underlying physics of the magnetostrictive phenomena and the state-of-the-art magnetostrictive patch transducers (MPTs) with various applications for nondestructive testing of waveguides.

Magnetostriction is a coupling phenomenon involving a magnetization process and dimension/shape change in ferromagnetic materials such as iron, nickel, and cobalt [1,2]. As illustrated in Fig. 1(a), a ferromagnetic material exhibits a change in its length (size) if it is subject to an external magnetic field. The size-changing effect is called the "Joule effect" [3]. On the other hand, the "Villari effect" [4] that is illustrated in Fig. 1(b) refers

* Corresponding author. Tel.: +82 2 880 7154; fax: +82 2 883 1513.
E-mail address: yykim@snu.ac.kr (Y.Y. Kim).
[1] Present address: Korea Institute of Nuclear Safety, 62 Gwahak-ro, Yuseong, Daejeon 305-338, Republic of Korea.

http://dx.doi.org/10.1016/j.ultras.2015.05.015
0041-624X/

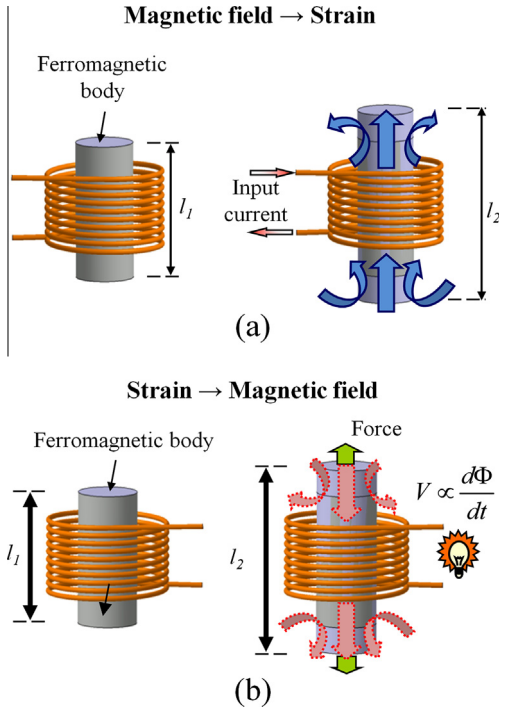

Fig. 1. Schematic descriptions of (a) Joule effect and (b) Villari effect.

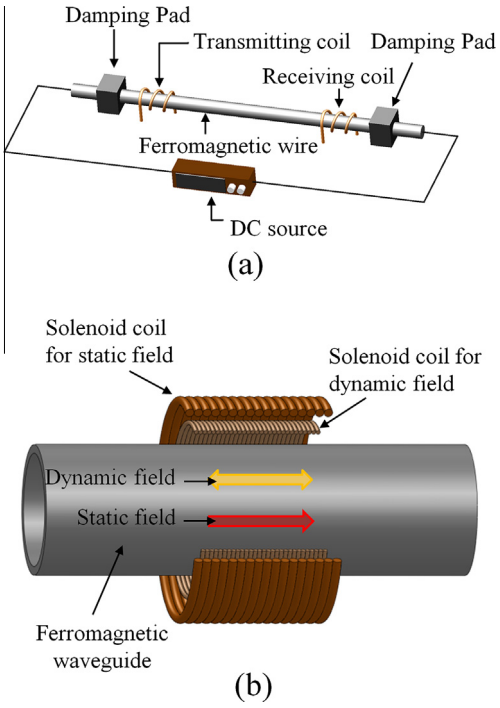

Fig. 2. (a) A setup to generate and measure a torsional wave in a ferromagnetic rod according to the Wiedemann and its reversed effects. (b) The generation and sensing of a longitudinal wave in a ferromagnetic pipe using magnetostrictive phenomena.

to the reverse phenomenon such that if there is any change in the length (size) of a ferromagnetic material, the material induces a magnetic field. When a ferromagnetic material is subject to a static magnetic field in one direction and a dynamic field from a direction orthogonal to the direction of the static field, a shearing deformation is developed in the material; this phenomenon is called the "Wiedemann effect" [5]. It was originally observed in a direct-current-flowing rod subjected to a time-varying longitudinal magnetic field as illustrated in Fig. 2(a); Fig. 2(a) is a sketch of the experimental setup that is used to measure a torsional wave in a rod, as depicted in [6]. The developed shearing deformation created by the Wiedemann effect results in a torsional wave in the rod. In this paper, all of these phenomena, whereby a magnetization process and mechanical deformation are coupled in a ferromagnetic material—either in sequence or *vice versa*—will be referred to as "magnetostrictive phenomena," unless there is a need to explicitly distinguish.

The first application of the magnetostrictive phenomena was possibly made in a magnetostrictive delay line [7,8] and the phenomena have been widely applied in the design of sensors that measure position, mass, field and others. (Refer to [9,10] for more comprehensive reviews on this subject.) The development of materials that exhibit strong magnetostrictive effects, such as Terfenol-D that is a giant magnetostrictive iron–terbium–dysprosium alloy [11], led to the popularity of actuators, transducers, and motors which were reliant upon magnetostrictive phenomena for their operation [12–15]. Studies on magnetostrictive-material characterization [16] and constitutive modeling [17–21] were also published.

Since magnetostrictive phenomena were used for the generation and measurement of guided waves [6,22,23], significant progress has been made in the development of magnetostrictive transducers which excite and measure guided waves for nondestructive testing (NDT) applications. Compared with other popular transducers used for NDT, such as piezoelectric transducers, magnetostrictive transducers have the following advantages: good sensitivity, durability, the absence of direct wiring to a transducer or test specimen, long-range inspection, easy implementation, and cost-effectiveness [24]. Since the operation of a magnetostrictive transducer involves a magnetic field for the generation and sensing of mechanical waves in a test specimen, it is often perceived as a kind of electromagnetic acoustic transducer (EMAT). In a non-ferromagnetic conductive material which is subject to a static bias magnetic field, an applied dynamic magnetic field induces the Lorentz force within it, thereby generating mechanical waves; the reversed mechanism of EMATs is used to sense elastic wave motions. In the case of a ferromagnetic material, an applied magnetic field induces magnetostriction as well as the Lorentz force, but magnetostriction is usually the dominant mechanism of ultrasonic wave transduction. In this paper, the term "EMAT" will be used to designate transducers that mainly use the operational Lorentz-force mechanism, while the transducers that mainly or solely use the operational magnetostrictive phenomena will be called "magnetostrictive transducers," unless stated otherwise.

In Figs. 2–4, a number of transducers and experimental settings that use magnetostrictive phenomena to generate and measure elastic waves in waveguides are schematically shown; in Fig. 2, elastic waves are generated and measured by the magnetostrictive phenomena of ferromagnetic waveguides. In Figs. 3 and 4, however, transducers that use thin magnetostrictive patches which are bonded onto or coupled with waveguides are shown; in these cases, the magnetostrictive effect and its reverse effect mainly occur in the patch. Elastic waves can therefore be excited and measured in both ferromagnetic and non-ferromagnetic waveguides if magnetostrictive "patch" transducers, as shown in Figs. 3 and 4, are employed. For convenience, magnetostrictive transducers with (Figs. 3 and 4) and without (Fig. 2) magnetostrictive patches will be denoted by "MPT" and "MsT," respectively.

While this paper is focused on MPTs, it is worth examining the development of MsTs because the operating principle is basically the same. Kwun and his colleagues pioneered MsT technology by demonstrating the generation and measurement of various wave

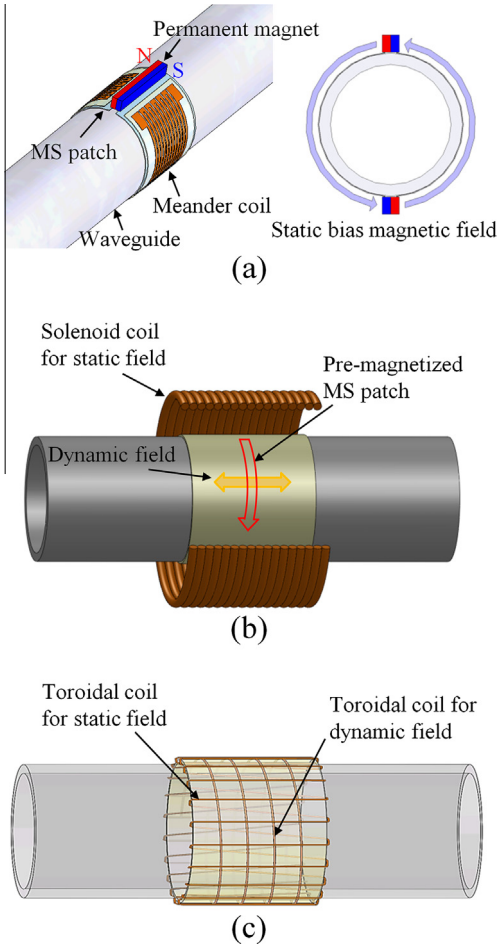

Fig. 3. Various configurations of magnetostrictive patch transducers (MPTs) that were developed to generate and measure torsional waves inside a pipe. The axial dynamic magnetic field is induced by the solenoid coil, while the circumferential static magnetic field is induced by (a) permanent magnets (© 2010 IEEE. Reprinted, with permission, from [57]), (b) pre-magnetization, and (c) a toroidal coil wound over the patch.

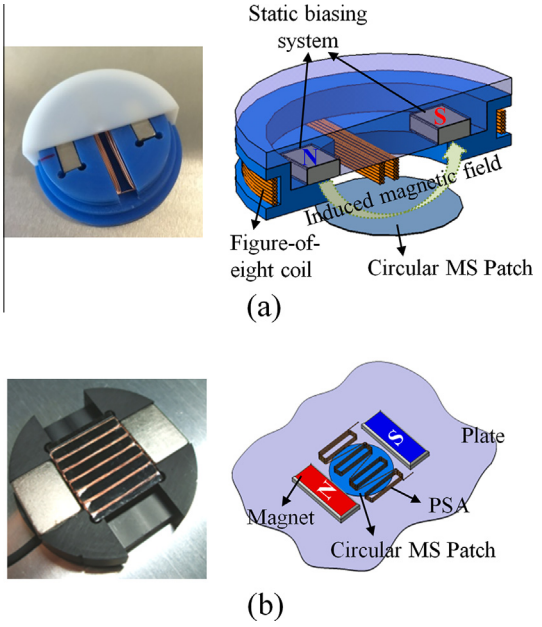

Fig. 4. Magnetostrictive patch transducers (MPTs) using (a) figure-of-eight coils (Reprinted with permission from [83]. Copyright 2007, AIP Publishing LLC) and (b) planar solenoid array (PSA) (from [84], © IOP Publishing. Reproduced by permission of IOP Publishing. All rights reserved.) for dynamic magnetic field generation. They are developed for the transduction of Lamb waves and/or shear-horizontal (SH)-guided waves in plates.

modes, ranging from longitudinal and flexural to torsional, in a steel rod [25]. They also developed MsTs for NDT of wire ropes, cables, strands, and pipes made of ferromagnetic materials [26–28]. The basic configuration of an MsT is illustrated in Fig. 2(b). It employs two solenoid coils, whereby one supplies a bias static field, and the other either provides a dynamic magnetic field to a waveguide or measures the induced magnetic field through the propagation of elastic waves in the waveguide. MsT applications include dispersion analysis in waveguides [29,30] and defect identification in steel pipes and tubes [31–34], steel plates with a T joint [35], and steel cables and strands [36–38]; a particularly interesting application is condition monitoring of an internal combustion engine [39]. Further developments of MsTs and their characterization were also reported [40–47] including measurement of bending waves or vibrations [48,49] and an attempt at MsT usage in a rotating shaft for crack detection [50]. The effectiveness of magnetostrictive transducers—especially for long-range ultrasonic inspections of steel waveguides—has been confirmed through the previously mentioned studies.

For an inspection of a non-ferromagnetic system or when a higher transduction efficiency is necessary in a ferromagnetic system, MPTs that employ magnetostrictive patches can be considered [51]. Some of the MPTs that have been developed for pipes/rods and plates are illustrated in Figs. 3 and 4. Because the patches are usually flexible, they can be easily installed on curved surfaces such as the cylindrical surfaces of pipes, and they can also be fabricated quite easily in any desired form. One of the most attractive features of patch MPTs is their effectiveness in the transduction of non-dispersive torsional (in a pipe) or shear-horizontal (in a plate) wave modes. Compare the complexity of patch-absent torsional wave generation (Fig. 2(a)) with the simplicity of magnetostrictive-patch generation (Fig. 3(a and b)); furthermore, complicated configurations are typically required to generate torsional wave modes with piezoelectric transducers [52,53]. Numerical wave simulations related to MPTs [54,55] and the equivalent-circuit modeling of an MPT [56] were also reported.

In terms of MPTs that were developed for the inspection of pipes/rods, longitudinal or torsional wave modes are the common MPT modes; several MPTs use the Wiedemann and its reverse effects for the transduction of torsional waves [24,57–60]. The performance improvement of MPTs is, however, an issue, so studies on mechanical impedance matching [61], magnetic flux concentration [62], and phased arraying for the selection of a specific mode [63] have been conducted. Various MPT applications were also reported for rotating shafts [64], wire ropes/cables and anchor rods [65], pipelines with mechanical attachments [66], pipes with axial cracks [67], and inspections of various defects and imaging [68–73]. In terms of inspection applications, a method that uses the Joule effect to generate torsional waves which can be applied for the inspection of rotating shafts [74] was proposed [75–77], while a pipe-inspection method that uses *in situ* magnetostrictive tapes and torsional waves was also suggested [78].

In terms of MPTs that were developed for plate applications, a significant advance has been made since the use of magnetostrictive patches for ultrasonic wave transduction in plates was first suggested [79,80]. Regarding plate applications, MPTs can generate directional [81–85] or omni-directional Lamb and shear-horizontal (SH) waves [86,87], and Fig. 4 shows some examples of directional MPTs. Plate-specific MPTs were not only used for imaging [88], but also for intriguing experiments involving phononic crystal and

metamaterial plates [89–91], while some modified plate-specific MPTs can be used to generate bulk SH waves [92,93]. The thin magnetostrictive patches used for plate-specific MPTs have also been used for elasticity modulus measurement [94] and structural health monitoring [95–97].

Sections 3 and 4 will present several types of MPTs that were developed for pipes (cylinders) and plates, along with their working mechanisms and applications. Because MPTs are mainly used to generate and measure waves that are propagated along waveguides, the underlying dispersion relations in waveguides will be briefly introduced in Section 2. The magnetostrictive principle, especially in the form of a linearized model, will also be presented in Section 2.

2. Fundamentals

2.1. Dispersion curves in waveguides

Because MPTs are developed to generate and measure strain/stress waves in waveguides such as plates, pipes, and rods, an understanding of wave-dispersion phenomena in guided waves is necessary. In the case of an isotropic plate of $2h$ thickness, the dispersion equations, where angular frequency is ω and wavenumber is k, are given as (e.g., [98,99]):

$$\sqrt{\frac{\omega^2}{c_L^2}-k^2}\times h=\frac{n\pi}{2}\quad (n:\text{integer})\ \text{for shear-horizontal waves,} \tag{1}$$

$$\frac{\tan(qh)}{\tan(ph)}=-\frac{4k^2pq}{\left(q^2-k^2\right)^2}\quad \text{for symmetric Lamb waves,} \tag{2a}$$

$$\frac{\tan(qh)}{\tan(ph)}=-\frac{\left(q^2-k^2\right)^2}{4k^2pq}\quad \text{for anti-symmetric Lamb waves,} \tag{2b}$$

where $p=\omega^2/c_L^2-k^2$ and $q=\omega^2/c_T^2-k^2$. The symbols c_L and c_T denote the longitudinal and shear-wave speeds, respectively.

Eqs. (1) and (2) yield an infinite number of wave modes including evanescent waves, but we are mainly concerned with non-decaying waves with real wavenumbers, as we are interested in the inspection of long-range guided waves. Figs. 5 and 6 show the dispersion curves for the SH and Lamb wave modes that are expressed as the relations between the group velocity c_g and the product of frequency and thickness ($f\times(2h)$ with $f=\omega/2\pi$). The mode numbers are denoted by SHn (SH waves), An (anti-symmetric Lamb waves), and Sn (symmetric Lamb waves),

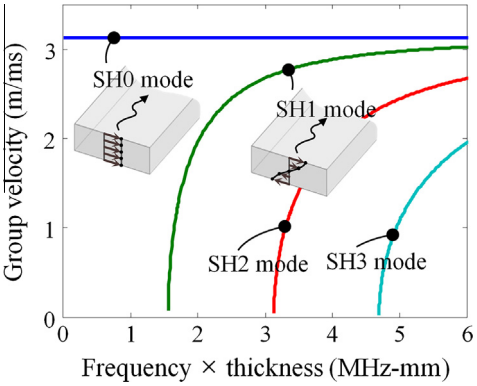

Fig. 5. Group velocity of the shear-horizontal (SH) wave for varying frequencies in an aluminum plate. Mode shapes of the lowest two modes (SH0 and SH1) in the thickness direction are also sketched.

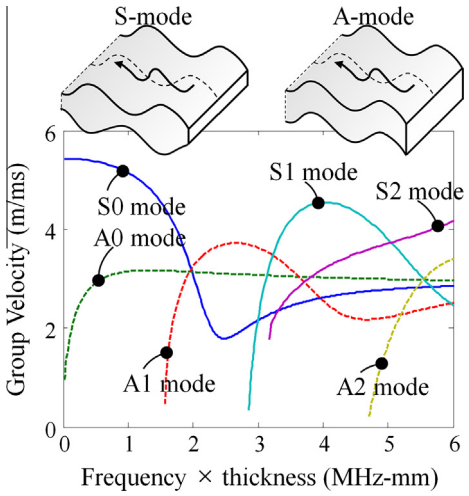

Fig. 6. Group velocity of the Lamb wave in an aluminum plate for the lowest three symmetric (S0, S1, S2) and anti-symmetric (A0, A1, A2) modes. Typical mode shapes of symmetric and anti-symmetric modes in the thickness direction are sketched.

with $n=0, 1, 2,\ldots$. Sketches of the mode shapes through the plate thickness are shown in the insets of the figures. From the dispersion curves, the cutoff frequencies f^c can be also found. As an example, f^c_{SH1} (the cutoff frequency for the SH1 mode) is 1.565 MHz in a 1 mm-thick plate, below which only the SH0 mode can propagate; likewise, only the SH0 and SH1 modes can propagate if an excitation frequency is lower than $f^c_{SH2}=3.13$ MHz.

The dispersion relation in a pipe of outer radius a and inner radius b can be similarly found (e.g., [100]). For instance, the dispersion relation for the torsional wave mode is given by

$$J_2(qa)Y_2(qb)-J_2(qb)Y_2(qa)=0, \tag{3}$$

where J_2 and Y_2 denote the first and second kinds of the Bessel function of order 2. The dispersion curve for torsional modes in a pipe is not plotted here because it is similar to the SH wave in a plate. As shall be shown, MPTs can effectively generate and measure torsional modes in a pipe including the lowest mode that is preferable for NDT of pipes.

2.2. Magnetostrictive phenomenon

As sketched in Fig. 7(a), an external magnetic field causes the rotation of magnetic domains in a ferromagnetic material, resulting in length change; this phenomenon is the Joule effect [3], whereas the reverse phenomenon is the Villari effect [4]. In a typical ferromagnetic material, the relation between the applied magnetic field H and the relative length change, i.e., strain ($S=\Delta L/L$), looks like the curve shown in Fig. 7(b). One peculiar phenomenon observed in the curve in Fig. 7(b) is that S has the same sign regardless of the sign of H; furthermore, the curves for most ferromagnetic materials are usually highly nonlinear. These issues must be properly addressed in designing a magnetostrictive transducer.

To generate mechanical waves in a ferromagnetic material using the Joule effect, a dynamic magnetic field (H_D) should be applied to a ferromagnetic material. If we assume that H_D oscillates around O at a frequency of ω_0, the dominant frequency of the generated mechanical wave would be $2\omega_0$, as illustrated in Fig. 7(c), because the sign of the generated wave is always the same. To achieve a linear response, a H_D value between $-\Delta H_D$ and $+\Delta H_D$ should be applied while the total field in a ferromagnetic material should be centered at point B that is located away from O; therefore, an appropriate static bias magnetic field H_S needs to be applied. Under the combined application of H_D and H_S, the time history of the resultant strain is sketched in Fig. 7(d). To ensure

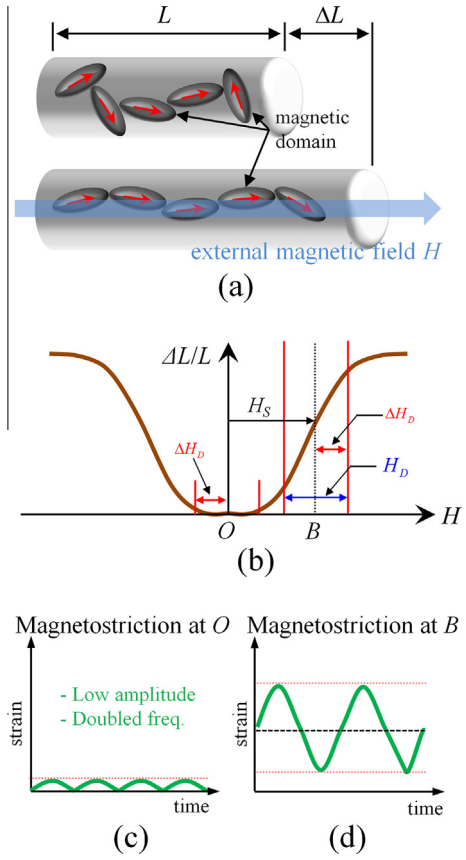

Fig. 7. (a) Schematic illustration explaining the Joule effect in a ferromagnetic material. (b) Typical magnetostrictive curve-related magnetic field (H) and mechanical strain ($S = \Delta L/L$). (c and d) Illustrative strain histories when time-vary magnetic fields (H_D) are applied at O and B, respectively.

linear behavior between the applied magnetic field and generated strain, ΔH_D must be sufficiently smaller than H_S. Optimal values of ΔH_D and H_S for efficient transduction may be found for selected magnetostrictive materials, desired wave modes, and transducer configurations. To increase transduction efficiency, compound materials such as Terfenol-D (an iron–terbium–dysprosium alloy; saturation magnetostriction = 1000–2000 ppm) and Hyperco 50A alloy (an iron–cobalt–vanadium soft magnetic alloy; saturation magnetostriction = 60–70 ppm) may be used, but Terfenol-D appears too brittle to be used as a base material for magnetostrictive patches in MPTs.

To understand the magnetostrictive behavior and derive a linearized magnetostrictive constitutive relation, we consider the unit volume of a magnetostrictive material under magnetic field vector $\mathbf{H}$ and stress tensor $\mathbf{T}$. If the resultant infinitesimal magnetic-flux-density vector and infinitesimal mechanical-strain tensor are denoted by $d\mathbf{B}$ and $d\mathbf{S}$, respectively, dU^{tot}, the change of the total internal energy of the infinitesimal volume, is [101]:

$$dU^{tot} = dU^{elastic} + dU^{magnetic} = \mathbf{T}^T d\mathbf{S} + \mathbf{H}^T d\mathbf{B}. \tag{4}$$

If an adiabatic condition is considered, the Gibbs free energy G_{MS} of a magnetostrictive material is written as:

$$G_{MS} = U^{tot} - \mathbf{T}^T\mathbf{S} - \mathbf{H}^T\mathbf{B}. \tag{5}$$

From Eq. (5):

$$dG_{MS} = dU^{tot} - d\mathbf{T}^T\mathbf{S} - \mathbf{T}^T d\mathbf{S} - d\mathbf{H}^T\mathbf{B} - \mathbf{H}^T d\mathbf{B}. \tag{6}$$

Substituting Eq. (4) into Eq. (6) yields:

$$dG_{MS} = -d\mathbf{T}^T\mathbf{S} - d\mathbf{H}^T\mathbf{B}. \tag{7}$$

Because strain components S_{ij} and magnetic flux components B_i can be expressed as $S_{ij} = -\partial G_{MS}/\partial T_{ij}$ and $B_i = -\partial G_{MS}/\partial H_i$, the following relation holds between strain and magnetic field and also between magnetic flux density and stress:

$$\frac{\partial S_{ij}}{\partial H_k} = \frac{\partial B_k}{\partial T_{ij}} = -\frac{\partial^2 G_{MS}}{\partial T_{ij}\partial H_k} \equiv d_{ijk} \qquad (i,j,k = 1,2,3), \tag{8}$$

where $\mathbf{d}$ is called the piezomagnetic coefficient. When a material exhibits magnetostrictive behavior, Eq. (8) states that there is always coupling between mechanical and magnetic fields. Therefore, $\mathbf{S}$ and $\mathbf{B}$ are functions of both $\mathbf{T}$ and $\mathbf{H}$, and can be written as:

$$dS_{ij} = \frac{\partial S_{ij}}{\partial T_{kl}} dT_{kl} + \frac{\partial S_{ij}}{\partial H_m} dH_m, \tag{9}$$

$$dB_i = \frac{\partial B_i}{\partial T_{jk}} dT_{jk} + \frac{\partial B_i}{\partial H_l} dH_l. \tag{10}$$

By using Eq. (8) and the definitions of compliance $\mathbf{s}$ (inverse of the elasticity tensor) and permeability $\boldsymbol{\mu}$, where $s_{ijkl} = \partial S_{ij}/\partial T_{kl}$ and $\mu_{il} = \partial B_i/\partial H_l$, one can write linearized magnetostrictive constitutive equations for small or infinitesimal changes in the field variables ($\mathbf{S}$, $\mathbf{T}$, $\mathbf{H}$, $\mathbf{B}$):

$$dS_{ij} = s_{ijkl} dT_{kl} + d_{ijm} dH_m \text{ or } d\mathbf{S} = \mathbf{s}d\mathbf{T} + \mathbf{d}^T d\mathbf{H}, \tag{11a, b}$$

$$dB_i = d_{ijk} dT_{jk} + \mu_{il} dH_l \text{ or } d\mathrm{B} = \mathbf{d}d\mathbf{T} + \boldsymbol{\mu} d\mathbf{H}. \tag{12a, b}$$

When the magnitude of the applied dynamic field is small compared with a static bias field, the following linearized constitutive relations, which result from Eqs. (11) and (12), can be used:

$$\mathbf{S}_D = \mathbf{C}\mathbf{T}_D + \mathbf{d}^T\mathbf{H}_D, \tag{13a}$$

$$\mathbf{B}_D = \mathbf{d}\mathbf{T}_D + \boldsymbol{\mu}\mathbf{H}_D, \tag{13b}$$

where the subscribed quantities with D are related to the applied dynamic magnetic field. In this case, the coefficients $\mathbf{C}$, $\boldsymbol{\mu}$, and $\mathbf{d}$ can be affected by the applied static bias field. Because the coupling coefficient $\mathbf{d}$ is the key material parameter governing the magnetostrictive phenomenon here, the effect of the static magnetic field on $\mathbf{d}$ must be considered for analysis. Also, $\boldsymbol{\mu}$ is determined from the nonlinear B–H curve, while it can be assumed that $\mathbf{C}$ is not affected by the applied magnetic field.

We will further examine the specific form of $\mathbf{d}$ for typical magnetostrictive materials that have been used to make thin magnetostrictive patches in MPTs, such as nickel (saturation magnetostriction = −35 to −50 ppm) and Hyperco. Assuming that a static uniform bias field H_S is applied along the x direction in a thin patch on the x–y plane (z: patch thickness direction), and that the applied dynamic field $\mathbf{H}_D$ is parallel or perpendicular to the static field in the x–y plane, the coupling coefficient $\mathbf{d}$ appearing in (13a) can be written in matrix form as [101]:

$$\mathbf{d} = \begin{bmatrix} d_{11} & d_{12} & d_{12} & 0 & 0 & 0 \\ 0 & 0 & 0 & 0 & 0 & d_{35} \\ 0 & 0 & 0 & 0 & d_{35} & 0 \end{bmatrix}. \tag{14}$$

In writing the components of $\mathbf{d}$ explicitly, we used shorthand notions (d_{ij} instead of d_{ijk}). The notation in (14) is consistent with the shorthand notations for tensor components, whereby $S_{ij} \iff S_I$ and $T_{ij} \iff T_I$ with $(ij) = (xx, yy, zz, yz, xz, xy) \iff (I) = (1, 2, 3, 4, 5, 6)$; also in (14), (x, y, z) are denoted by $(1, 2, 3)$ for components of $\mathbf{B}$ and $\mathbf{H}$. As a consequence of these shorthand notations, the contents of Eq. (13) are treated as matrix equations. The components of Eq. (14) are defined as [102]:

$$d_{11} = \left.\frac{\partial f(H)}{\partial H}\right|_{H_S}, \quad d_{12} = -0.5 d_{11}, \quad d_{35} = 3\frac{F(H_S)}{H_S}, \tag{15}$$

where F is a function describing the one-dimensional magnetostrictive relation between H and S that is usually determined experimentally.

By examining Eqs. (13) and (14), the following observations can be made: If a dynamic magnetic field $(H_D)_x$ is applied to a magnetostrictive patch in the direction parallel to the static bias field $(H_S)_x$, the normal strain components S_{yy} and S_{zz} (the S_{zz} shown in a thin patch in Fig. 4 can be ignored) are also generated in addition to S_{xx} due to the non-zero value of d_{12}. Alternatively, if the applied dynamic magnetic field $\mathbf{H}_D$ is in the y direction (i.e., $(H_D)_y \neq 0$) under a static bias field in the x direction, non-vanishing shear strains (e.g., $S_{xy} = S_6$) are developed in the patch. Usually known as the Wiedemann effect [5], this phenomenon of shear-strain generation in a magnetostrictive patch can be used to generate SH waves or torsional waves when it is bonded onto a plate or a pipe. When $\mathbf{H}_D$ is neither parallel nor perpendicular to the direction of the static magnetic field, both shear and normal strains will be generated. A detailed analysis for such a case was given in [55,103,104]. Understanding these basic mechanisms is important for the design of various MPTs, as demonstrated in the subsequent sections.

3. MPTs for NDT applications in pipes and rods

This section reviews MPTs that were developed for applications in pipes and rods. First, we noted that among longitudinal, bending, and torsional-guided wave modes in pipes and rods, the torsional wave mode appears to be an attractive wave mode for NDT applications; the lowest torsional mode is non-dispersive and its propagation is largely unaffected by liquid content in pipes. While MPTs can be used to excite all types of guided modes, they are most widely used to generate the torsional wave of a considerable power because the use of popular piezoelectric transducers to generate this type of wave would require complicated settings. Most of the discussions here will therefore be focused on torsional-wave-mode generation, even though MPTs can also generate longitudinal and flexural wave modes.

Because torsional waves involve a shearing deformation, we first consider the Wiedemann effect of magnetostrictive patches for torsional wave generation. Fig. 3 shows three MPT configurations that can be used to generate torsional waves. Typically, a dynamic magnetic field along the axial (longitudinal) direction is supplied to the patch by a solenoid coil encircling the patch. In terms of a static magnetic field in the circumferential direction, it can be applied to the patch using three different methods: permanent magnets, as depicted in Fig. 3(a); the pre-magnetization shown in Fig. 3(b); and the toroidal coil of Fig. 3(c). In all configurations in Fig. 3, the static circumferential and the dynamic axial magnetic fields are superposed to generate shearing deformation in the patch by the Wiedemann effect. The shearing deformation of the patch, in turn, induces a torsional wave in the test pipe. The main difference among the three configurations in Fig. 3 is the method of supplying a circumferential static magnetic field to the patch. For this section, the MPT in Fig. 3(a) and its modifications will be mainly focused, but the MPTs illustrated in Fig. 3(b and c) will be first discussed.

In all configurations, a magnetostrictive patch is bonded to a pipe surface with epoxy or coupled by shear couplant with a test pipe. When epoxy is used for patch bonding, a method to ensure a sound adhesion should be considered. The simplest method is to put a weight in the range of a few kilograms on a patch that is bonded to a plate, or to use sellotape to ensure firm bonding between a patch and a cylinder or pipe. The use of shear couplant is often preferred as a means to couple an MPT with a test plate or pipe when the same transducer needs to be used at several different locations. Although the wave transmission from the patch to a waveguide during coupling with shear couplant might not be as good as the transmission when bonding with epoxy, the former is comparable with the latter in most applications. We used Sonotech SHEAR GEL® MAGNAFLUX as a shear couplant in our experiments [63,91,93].

The transducer in Fig. 3(b) is actually the first MPT used specifically for pipe applications; it was developed by Kwun et al. [24], who used a circumferentially pre-magnetized, strip-type magnetostrictive patch. For pre-magnetization, the patch is rubbed with a permanent magnet before its installation on a pipe, whereby the residual magnetization is exploited. (If the patch is pre-magnetized along the axial direction in a pipe, a longitudinal wave instead of a torsional wave is generated.) Some successful applications of this method for structural condition monitoring and its improvement were reported in [64,66,69].

Alternatively, a toroidal coil encircling the patch can be wound [58,59,105] to supply a static field with DC current as suggested in Fig. 3(c), This way, a strong and magnitude-adjustable bias magnetic field can be applied. The relative magnitude of the dynamic magnetic field may therefore be controlled to achieve the most effective wave transduction; however, the fabrication of the MPT could be somewhat cumbersome and an elaborate effort is required in cases of tight coupling with a test pipe.

For the long-term, cost-effective installation of MPTs on a pipe for vibration testing, Cho et al. [106] proposed the installation of permanent magnets and pointed out that MPTs equipped with magnets can generate large actuation power stably and effectively. The MPT configuration shown in Fig. 3(a) was developed in [57], and the first successful generation and measurement of torsional waves in a megahertz frequency range was reported. To generate megahertz torsional waves, a meander coil was incorporated into the MPT design. Each "finger" of the coil was separated by half the wavelength of a target-frequency. Additionally, the installed permanent magnets provided a stable bias magnetic field for the strip-type magnetostrictive patch, so a greater quantity of permanent magnets may therefore be needed for larger pipes.

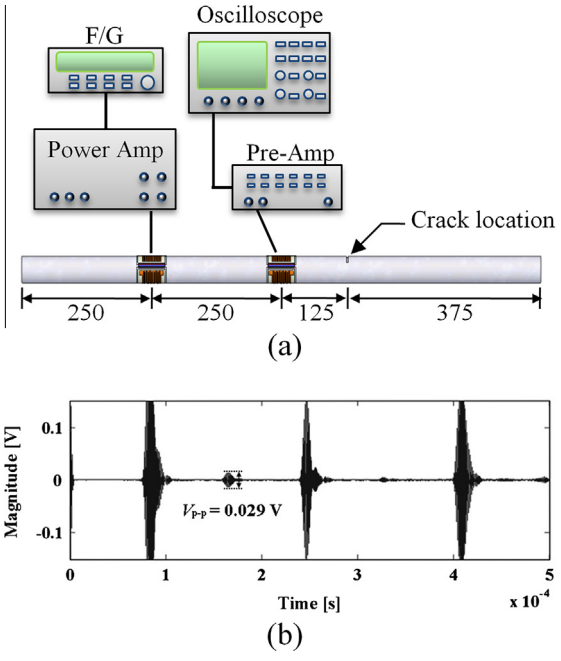

Fig. 8. (a) Experimental setup for crack detection by a magnetostrictive patch transducer (MPT) using a torsional wave pulse centered at 1 MHz in a pipe and (b) the measured signal. (© 2010 IEEE. Reprinted, with permission, from [57].)

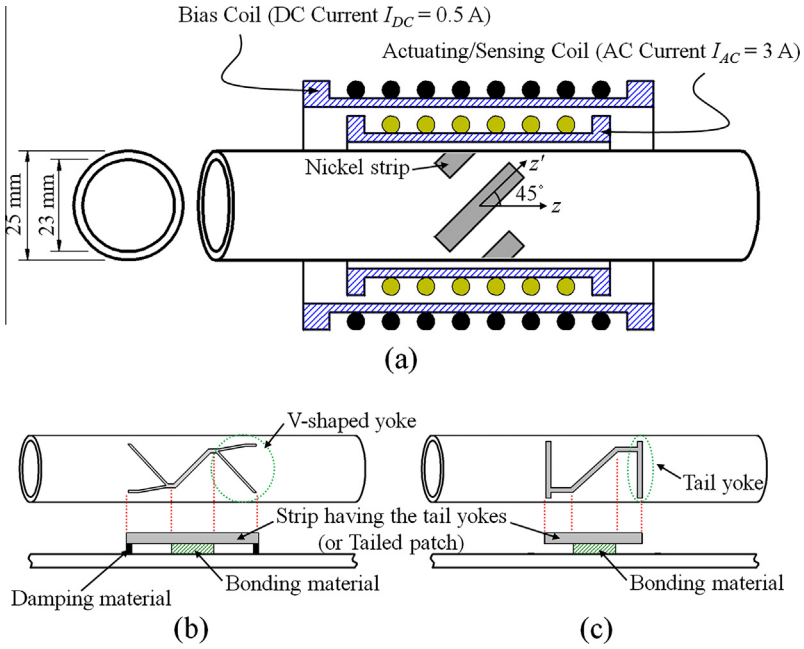

Fig. 9. (a) Illustration of a torsional-wave magnetostrictive patch transducer (MPT) using magnetostrictive strip-patches with the alignment angle of 45° relative to the pipe axis (proposed in [76]). Modifications using (b) the V-shaped yokes (Reprinted with permission form [77]. Copyright 2005, AIP Publishing LLC) and (c) the tail yokes. (Reprinted with permission form [78]. Copyright 2006, AIP Publishing LLC.)

The performance of the MPT in Fig. 3(a) was tested to detect a crack (width: 0.4 mm, cross-sectional area ratio: 2%) that was artificially made in a stainless steel tube (diameter = 25 mm, thickness = 1 mm, length = 1000 mm). The experimental setup is shown in Fig. 8(a) and the measured signal using the same MPT receiver is shown in Fig. 8(b). For the experiment, the torsional wave at the center frequency of 1 MHz was used. (See Appendix A for a more detailed experimental procedure.) Because the lowest mode is non-dispersive, all of the pulses recorded in Fig. 8(b) are virtually undistorted. The pulses that appeared at 0.08 and 0.25 ms denote the direct wave from the transmitter and the reflected wave from the left end, while the pulse appearing at 0.16 ms is the reflected wave from the crack, which would be difficult to detect if a lower-frequency wave (e.g., 150 kHz wave) had been used. Further to the previously mentioned application, the magnet-installed MPTs that use torsional waves were also successfully used for pipe imaging [71,72], wall-thinning detection [107], and axial crack detection [67].

Most of the MPTs for torsional waves including those sketched in Fig. 3 operate in accordance with the Wiedemann effect and its reverse effect; however, by installing magnetostrictive patches of MPTs at certain angles relative to the longitudinal axis, it is still

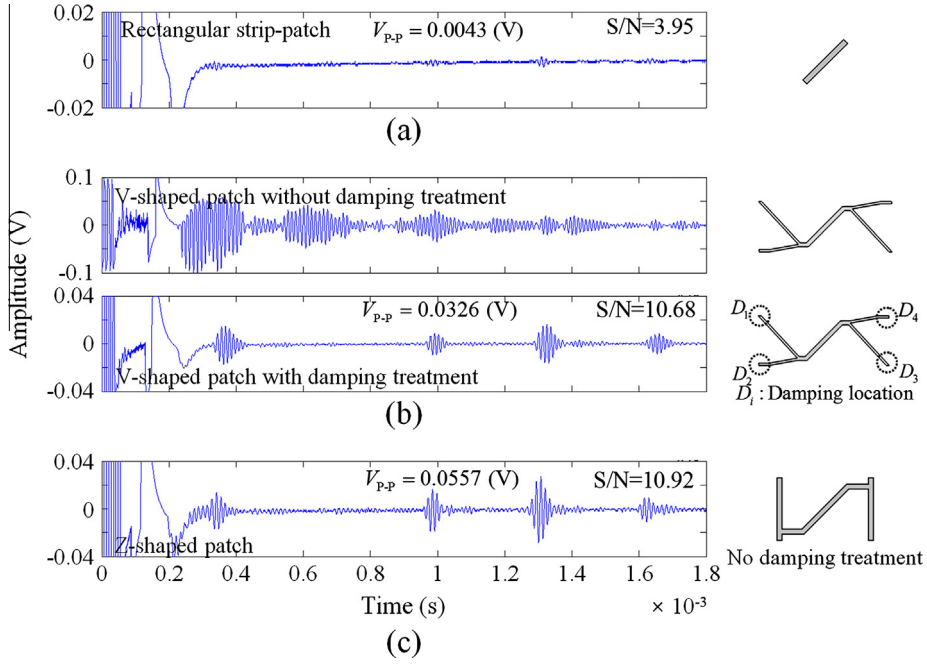

Fig. 10. Voltage signal measured by the solenoid. The results with (a) a set of oblique magnetostrictive (MS) strips without any yoke [76], (b) a set of strip-patches with V-shaped yokes [77], and (c) a set of the Z-shaped patches [78]. (Reprinted with permission form [78]. Copyright 2006, AIP Publishing LLC.)

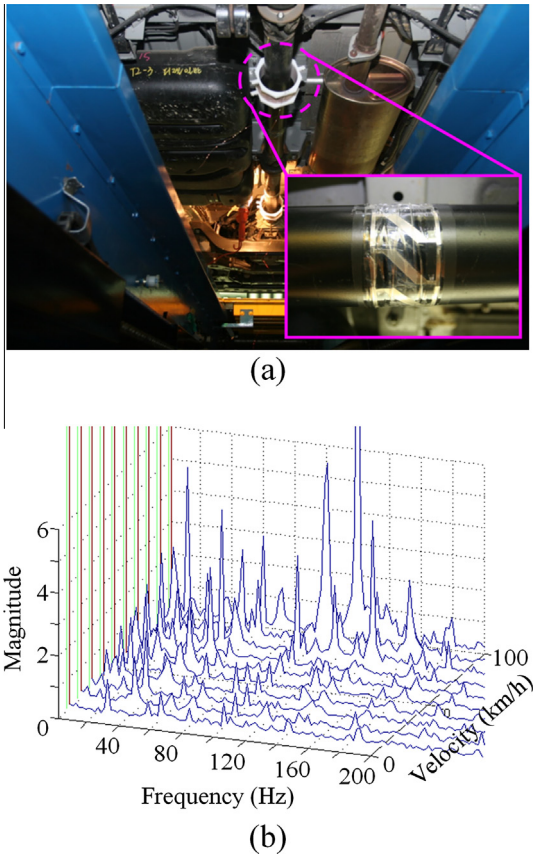

Fig. 11. (a) Z-shaped magnetostrictive patch transducer (MPT) installed on the propeller shaft of a rear-wheel-drive van for torsional vibration measurement and (b) waterfall diagrams of vibration signals with varying vehicle speeds.

possible to also generate and measure torsional waves by the Joule/Villari effects. The three configurations developed so far, including the inaugural development in Fig. 9(a), are shown in Fig. 9 [75]. Compared with the MPT configurations shown in Fig. 3, the MPTs in Fig. 9 can be used not only in stationary pipes, but in rotating shafts as well. The configurations in Fig. 3(a and c) cannot be used in a rotating shaft because wiring to the MPT coils interferes with shaft rotation. The configuration in Fig. 3(b) that requires pre-magnetization could be used for a rotating shaft, but the issue of the de-magnetization and re-magnetization of the patch bonded onto the shaft must be properly addressed. The application of the MPT in Fig. 9 was demonstrated in [74], in which only a few thin strip-type patches were bonded on a rotating shaft.

To explain the mechanism of the Joule-effect torsional wave generation in the MPT shown in Fig. 9(a), it is noted that the strip-shaped patches under both the static and dynamic magnetic fields supplied by the two solenoid coils would be deformed mainly along the 45° z' axis. (In [108], it was found that a strip-orientation angle slightly less than 45° is more effective.) If the generated normal strain $\varepsilon_{z'z'}$ relative to the primed coordinate system is transformed into the z–θ coordinate system (where θ is the circumferential direction), the resultant field would be dominated by the shear stress component $\varepsilon_{\theta z}$ that generates torsional waves in the shaft.

The transduction efficiency can be substantially increased if the patches shown in Fig. 9(b) [76] and Fig. 9(c) [77,103] are used. In Fig. 9(b), two V-shaped yokes connected to the central, slender strip-type patch serve to concentrate the applied magnetic fields using the solenoids on the patch. The V-shaped yokes are not bonded or coupled with a test structure because they should not

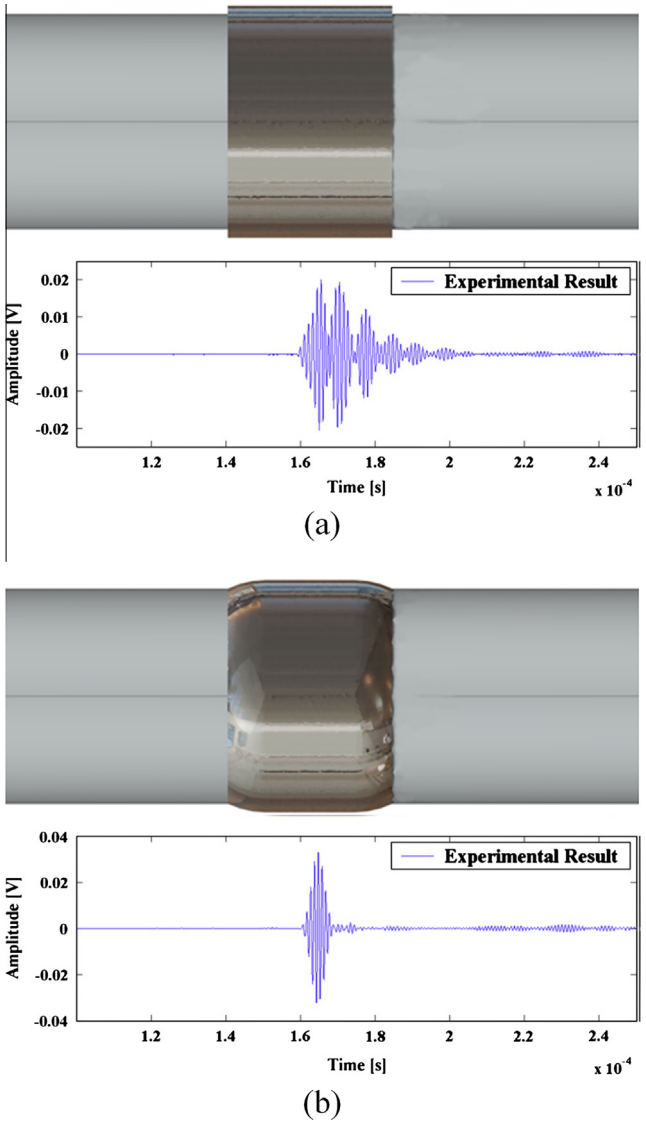

Fig. 12. Photos of the magnetostrictive patches of torsional magnetostrictive patch transducers (MPTs) using a 3-turn meander coil and the measured signals in an aluminum pipe. (The center frequency is 1 MHz.) The results (a) before and (b) after acoustic impedance matching. (Reprinted from [62], Copyright (2011) with permission from Elsevier.)

contribute to the induction of any strain in a test structure; instead, they should function only as magnetic paths. A further improvement is the Z-shaped patch (simply called the "Z-patch") shown in Fig. 9(c). Also in this patch configuration, only the obliquely-arranged central part of the Z-patch is bonded onto a test structure because the remaining part only serves to concentrate the magnetic field; the shape and suggested partial bonding state of the Z-patch were found to be optimal as confirmed by the topology optimization method [103].

To check the performance of the MPTs' torsional wave generation that is shown in Fig. 9, pitch–catch torsional wave experiments were performed in an aluminum pipe (outer diameter = 25 mm; wall thickness = 2 mm) and the results comparison is presented in Fig. 10. A comparison of Fig. 10(a and b) shows that, while the use of a patch equipped with V-shaped yokes produced larger signals than those of the simple oblique strip-type patch, the structural vibration of the yokes induced the generation of undesired wave modes. Interestingly, Fig. 10(b) also shows that undesirable vibrations disappear if damping materials are used to

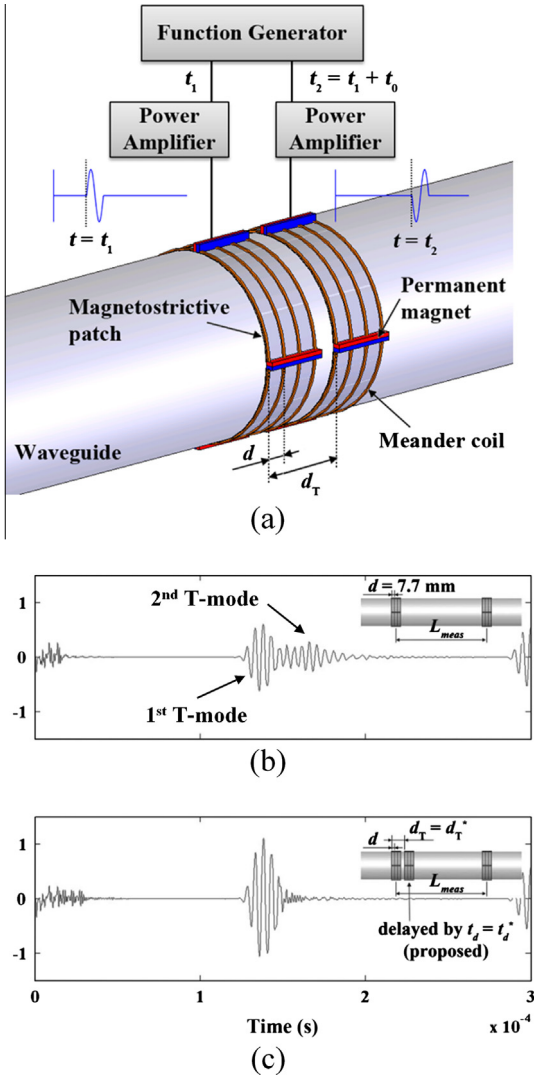

Fig. 13. (a) Two magnetostrictive patch transducers (MPTs) used to form an array transducer. Each MPT employs a 4-finger meander coil. Experiments performed in an aluminum pipe with torsional wave pulse centered at 200 kHz. The results in (b) and (c) show the measured signals by a single MPT and an array of two MPTs, respectively. (© 2013 IEEE. Reprinted, with permission, from [64].)

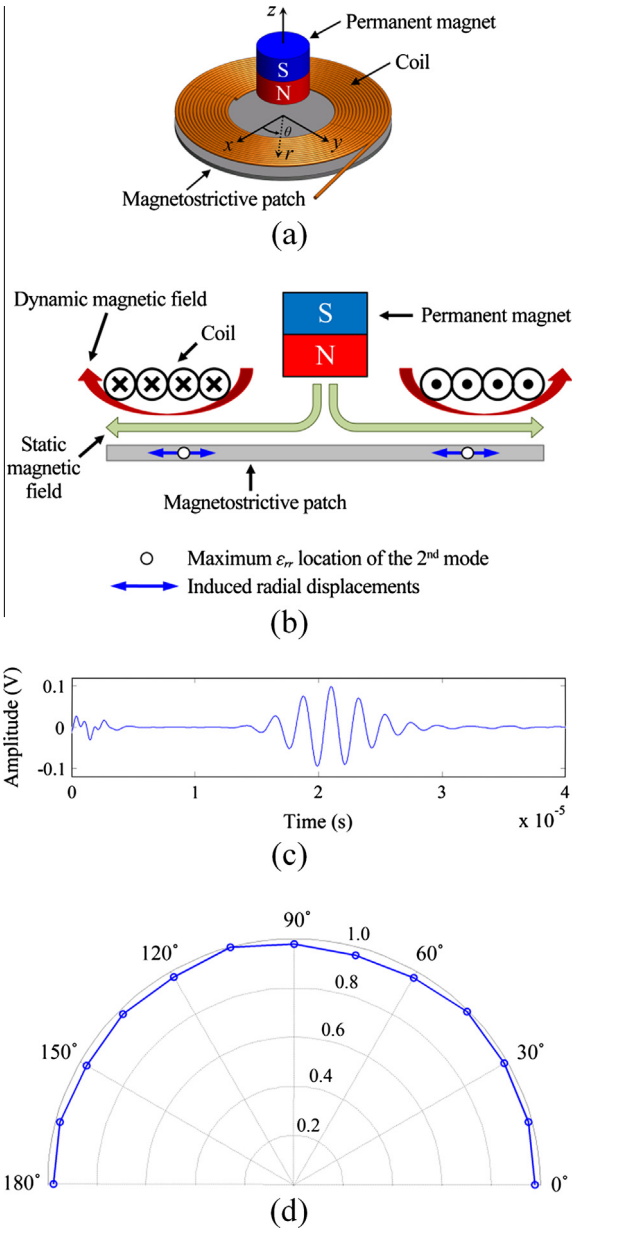

Fig. 14. (a) Magnetostrictive patch transducer (MPT) for omni-directional Lamb waves in a plate as proposed. (b) Schematics of static and dynamic magnetic fields induced by a permanent magnet and coil. (c) Measured signal from MPT for an excitation Gabor pulse of 430 kHz. (d) The radiation pattern of the MPT (© 2013 IEEE. Reprinted, with permission, from [87].)

treat the end parts of the V yokes. On the other hand, the MPTs that employ Z-patches, called "Z-MPTs" in this paper, generate and measure torsional waves with larger magnitudes and higher signal-to-noise ratios without needing to undertake the somewhat cumbersome damping treatment; see Fig. 10(c).

As pointed out earlier, one interesting application of the torsional Joule-effect MPTs is their use in torsional wave/vibration experiments that are conducted in rotating shafts. As direct wiring to Z-patches is not needed, the Z-MPT can be used for a rotating shaft. Also, the Z-MPT uses a solenoid coil that encircles a rotating shaft, so the output signal from a Z-MPT will not be significantly influenced by the lateral vibrations affecting the solenoid fill factor. Fig. 11(a) shows a photo of a Z-MPT installed on the propeller shaft of a rear-wheel-drive van [109]. The transducer was used to measure torsional vibrations of the shaft while it was rotating; as measurements should be made during shaft rotation, the wireless characteristic of the Z-MPT is crucial here. The solenoid coil encircling the Z-patches that are bonded on the shaft is installed in the automobile subframe. The waterfall plot of the vibration signals for varying vehicle speeds is shown in Fig. 11(b). A further analysis of the measured signals indicated that the torsional vibrations were captured correctly although some bending vibrations were also sensed.

Returning back to the MPT applications in pipes, it is worth mentioning a few more studies. If high-frequency torsional waves in a range of megahertz frequencies need to be generated by torsional MPTs, impedance matching at the interface between the bare part and the magnetostrictive patch-bonded part of a test pipe should be considered to avoid any distortion of the generated waves [61]. Fig. 12(a and b) shows the generated wave signals before and after impedance matching treatment. The treatment simply machined small-end regions of the patch for smooth–thickness variations because internal reflections within the patch are responsible for wave distortion.

So far, the torsional MPTs were used at frequencies below the first cutoff frequency. For NDT inspections of smaller defects, the use of the lowest non-dispersive torsional mode at a higher frequency above the first cutoff frequency can be effective. Kim et al. [63] presented a method to use two torsional MPTs. The distance (d_T) and time delay (t_d) between them were simultaneously adjusted so that the higher mode was rejected and only the lowest mode was transmitted. Fig. 13(a) shows two torsional MPTs, each of which employs 4-finger meander coils that are installed on a 13 mm-thick test pipe with a pipe cutoff frequency of 120 kHz. In Fig. 13(b and c), the experimental result obtained with a single torsional MPT at 200 kHz is compared with the results of the two torsional MPTs with $d_T = t_d \times c_{g_2}$ and $t_d = \lambda_2/(c_{p_2} - c_{g_2})$, where c_{p_2} and c_{g_2} respectively denote the phase and group velocities of the second torsional mode at a test frequency of 200 kHz [63], respectively. Fig. 13(c) confirms the effectiveness of using two MPTs with adjusted d_T and t_d for the generation of only the lowest torsional wave mode.

4. Plate-specific MPTs for NDE applications

Since the possibility of using the magnetostrictive principle for ultrasonic wave transduction in plates was reported by Kwun et al. [79,80], several kinds of plate-specific MPTs have been developed. The currently-available plate MPTs may be divided into two types, omni-directional and directional, depending on the directivity of the MPT-generated waves. The omni-directional MPTs shown in Figs. 14(a) and 15(a) were developed to generate omni-directional Lamb waves [86] and omni-directional SH waves [87], respectively. Fig. 4 shows the directional MPTs that were designed to transmit the Lamb or SH waves dominantly along desired wave directions.

Starting with omni-directional MPTs, the omni-directional Lamb-wave MPT in Fig. 14(a) (subsequently referred to as "OL-MPT" in this paper) is axisymmetrically configured. It consists of a circular magnetostrictive patch, a cylindrical magnet placed over the patch center with some distance, and a planar solenoid coil. In Fig. 14(b), the sketches show the magnet and coil producing radially-flowing static and dynamic magnetic fields in the circular patch, respectively. A signal measured during a pitch–catch experiment on a 2 mm aluminum plate is plotted in Fig. 14(c) and, for the experiment:

- two OL-MPT's were located 100 mm apart from each other,
- the circular patches of the MPTs of 0.15 mm in thickness and 20 mm in diameter (D) were bonded onto a plate by epoxy,
- the hollow circular coil was made of an enamel-coated wire of a 0.3 mm diameter,

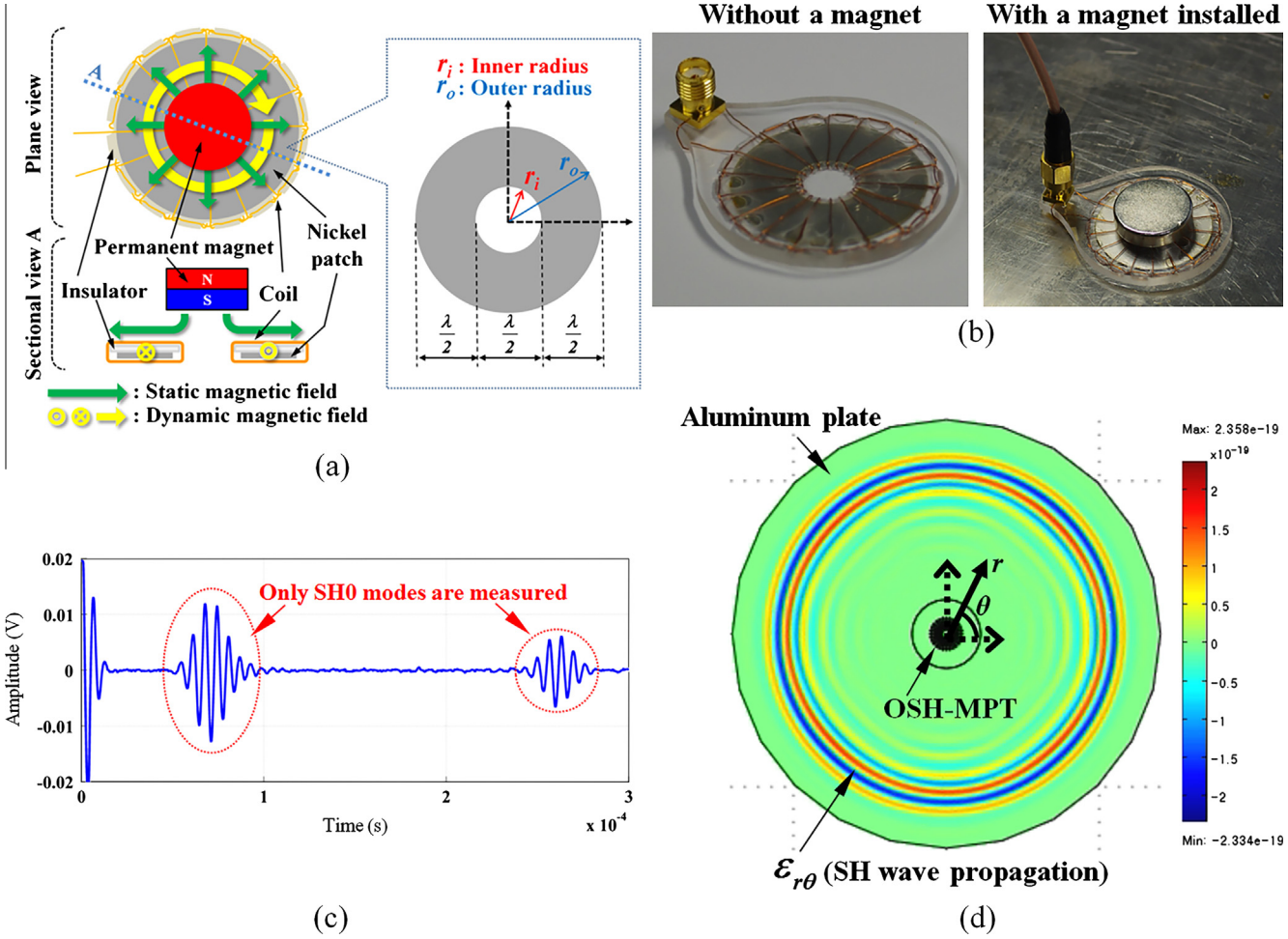

Fig. 15. (a) Schematic drawing of magnetostrictive patch transducer (MPT) for transduction of omni-directional shear-horizontal (SH) waves in a plate. Magnetic field directions in the patch by the coil and the magnet are also illustrated. (b) Photos of the fabricated MPT with and without a permanent magnet installed. (c) Measured signal of the generated Gabor pulse centered at 150 kHz. (d) Snapshot of the shear-strain component ($\varepsilon_{r\theta}$) in an aluminum plate at t = 35 μs. The radial and circumferential directions are denoted by r and θ, respectively. The SH Gabor pulse at 150 kHz was excited by the MPT located at the center of the plate. (Reprinted from [88], Copyright (2013) with permission form Elsevier.)

- the outer diameter of the coil was D while its inner diameter was $D/2$,
- the Gabor pulse (see Appendix A) centered at 430 kHz was used as the input signal.

Note that the measured signal in Fig. 14(c) contains no other guided wave mode except the S0 Lamb wave mode. The patch and coil sizes were deliberately determined to excite and measure the desired S0 mode in the most efficient manner; among others, the wavelength of the second in-plane eigenmode of a freely vibrating magnetostrictive patch of diameter D was matched with the wavelength of the target S0 Lamb-wave mode of the test plate [86]. The omni-directivity of the OL-MPT can be confirmed, as shown in Fig. 14(d).

Fig. 15(a) shows the configuration of the MPT that was designed to generate omni-directional SH waves alongside sketches of magnetic field directions, while Fig. 15(b) shows photo images of the transducer; the transducer will subsequently be referred to as the "OSH-MPT." As shown in Fig. 15(a and b), the OSH-MPT consists of an annular magnetostrictive patch, a cylindrical permanent magnet, and a coil positioned over the patch [87] that is specially wound in the form of a toroidal coil. The magnet supplies a radial bias magnetic field and the circumferential dynamic magnetic field of the coil to the patch, as shown in the sketches of Fig. 15(a); this transducer is therefore operated by the Wiedemann effect. To maximize the transduction efficiency of the OSH-MPT, its annular width $(r_o - r_i)$ should be equal to half the wavelength of the desired SH0 mode [87]. Fig. 15(c) shows that only the SH0 wave mode was excited and measured by the OSH-MPT. The Gabor pulse similar to the one used for the experiments with the OL-MPT was the input signal. As it is difficult to generate pure, omni-directional SH wave modes of a sufficient strength when using other transducers, the successful generation of SH wave modes through the use of the magnetostrictive principle should be further explored for various applications. The simulation result that confirms the omni-directivity of the OSH-MPT is shown in Fig. 15(d) with a snapshot of the plotted shear-strain component. The experimental results in [87] confirm the omni-directivity.

To transmit guided waves in a plate mainly along a target direction, the MPTs[2] [81–83] shown in Fig. 4 can be used. These directional MPTs also use circular magnetostrictive patches, but the magnetic circuits are different from those used for the omni-directional MPTs. In the case of the directional MPT in Fig. 4(a), the angle (θ) between the direction of the bias magnetic field of two magnets and the direction of the dynamic field of a figure-of-eight coil can both be adjusted; the angle affects the type and magnitude of generated wave modes, and in turn, the radiation patterns of a directional MPT.

An experimental setup with directional MPTs is described in Fig. 16(a), while Fig. 16(b and c) present the radiation patterns of the S0 Lamb and SH0 wave modes when the transmitters of $\theta = 0°$ ($H_s // H_D$) and 90° ($H_s \perp H_D$) are used, respectively. For the plots, pitch–catch experiments were performed with the Gabor pulses centered at 300 kHz as the input signals. These figures show that the S0 and SH wave modes are transmitted dominantly along the directions of the dynamic magnetic field when $\theta = 0°$ (see Fig. 16(b)) and $\theta = 90°$ (see Fig. 16(c)); however, they are always accompanied by the other modes. For example, in the case of $\theta = 0°$, the transducer generates the dominant S0 mode along the direction parallel to the dynamic field (indicated by the $\alpha = 0°$ direction), but it also generates the SH0 mode dominantly along the direction of $\alpha = 45°$; the case of $\theta = 90°$ exhibits similar behavior. For an MPT to be a truly directional transducer, it should independently generate the S0 or SH wave modes; however, it is not possible to transmit only the desired mode with this configuration because the strain field is a tensor field. A shear-strain field related to other coordinate axes always exists, even if a strain state at a point is dictated only by normal strain components relative to certain axes, and *vice versa*. This observation can be confirmed immediately because the radiation pattern of the transducer-derived SH0 mode of $\theta = 0°$ in Fig. 16(b) is the same as that of the transducer-derived S0 mode of $\theta = 90°$. To overcome this limitation and reduce the width of the generated wave beam, the transducer in Fig. 4(b) can be used.

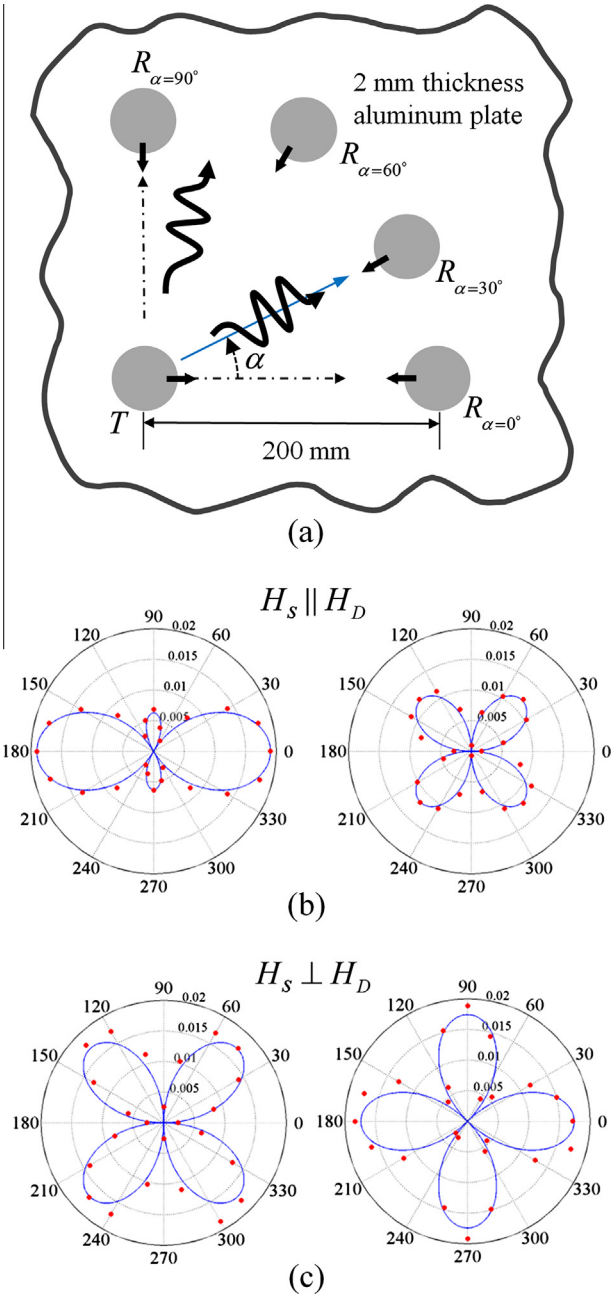

Fig. 16. (a) Schematics for experiments to find the radiation patterns of the magnetostrictive patch transducer (MPT) shown in Fig. 4(a). Measured radiation patterns for the excitations when the dynamic (H_D) and static (H_S) magnetic fields are (b) parallel and (c) perpendicular to each other. In (b and c), the left and right figures denote the radiation patterns of the Lamb and shear-horizontal (SH) waves.

[2] They were called OPMT's in earlier works, but they will be called MPT's in this paper for consistency.

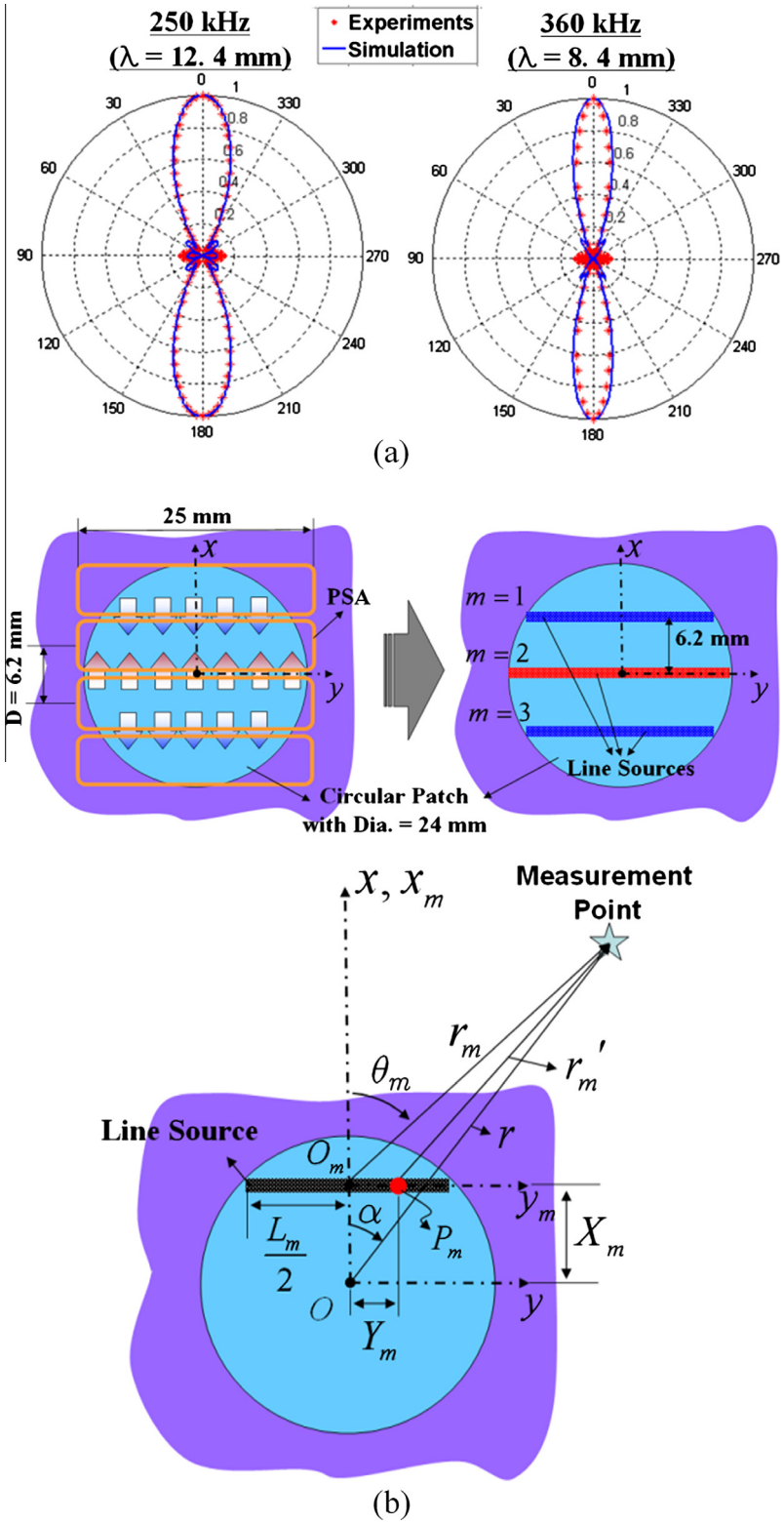

Fig. 17. (a) Radiation patterns of the generated SH waves by the magnetostrictive patch transducer–planar solenoid array (PSA–MPT). The center frequencies of the input Gabor pulses are 250 and 360 kHz. (b) The analytic model used to predict the radiation pattern. The magnetic field distributions in the magnetostrictive patch are illustrated for the PSA of $N = 5$ and $D = 6.2$ mm. (From [84], © IOP Publishing. Reproduced by permission of IOP Publishing. All rights reserved.)

The key for the transducer shown in Fig. 4(b) is the use of a Planar Solenoid Array (PSA) [83] and the MPT using the array will subsequently be called "PSA–MPT" in this paper. Note that each planar solenoid is formed by multiple turns of wires. In particular, Fig. 4(b) illustrates a PSA–MPT in which the angle between the static and magnetic field directions is $\theta = 90°$. If $\theta = 90°$, the PSA–MPT generates and measures a beam-focused SH wave mode. Similarly, one can also make a PSA–MPT to generate a beam-focused Lamb-wave mode by choosing $\theta = 0°$. The distance between the centers of planar solenoids in the PSA should be

adjusted to be half the wavelength of the target wave mode at an excitation frequency. Consequently, the interference among the waves generated by multiple planar solenoids becomes constructive among the desired wave modes so that a desired mode with a narrow beam size can be generated. A minimum of three planar solenoids was needed to achieve the goals. The radiation patterns of the PSA–MPT-generated SH0 waves at two different frequencies are shown in Fig. 17(a). The radiation patterns of the PSA–MPT can be accurately predicted by using a first-order theory in accordance with the line-source model depicted in Fig. 17(b). The horizontal lines appearing in the upper-right sketch in Fig. 17(b) denote the segments of the circular patch that experienced dominant shear deformation due to the applied magnetic fields. Using the line-source model depicted in Fig. 17(b), the signal magnitude $R(r, \alpha, t)$ picked up by a receiving transducer can be accurately predicted as [83]:

$$R(r,\alpha,t) = A_0\sqrt{\frac{2}{\pi}}e^{-j\left(\omega t-\frac{\pi}{4}\right)}\sum_{m=1}^{N-1}(-1)^m \times \frac{L_m}{\sqrt{r_m}}\left[\frac{\sin\left(\frac{1}{2}kL_m\sin\theta_m\right)}{\frac{1}{2}kL_m\sin\theta_m}\right]e^{jkr_m}, \tag{16}$$

where $r_m = \sqrt{(r\sin\alpha)^2 + (r\cos\alpha - X_m)^2}$ and $\theta_m = \tan^{-1}[r\sin\alpha/(r\cos\alpha - X_m)]$. The definition of r and α can be found in Fig. 17(b), and N denotes the number of planar solenoids. The theoretical results in Fig. 17(a) were calculated using Eq. (16).

Due to the unwanted mode rejection capability and narrow-beam generation capability of the PSA–MPTs, they can be useful in various applications including imaging. In Fig. 18, the experimental setup [88] and processed images for the detection of two 1-mm hole cracks in a 0.8 mm aluminum plate using the SH0 mode at 360 kHz are shown. We only used a total of four transducers, where one transducer works as a transmitter while the three remaining transducers work as receivers. The rectangular region of the inspection occupying (10, 30) × (10, 30) (unit: cm) was discretized by N_P grid points that the transducers were focused on. For the experiment, the transducers were located at (0, 0), (0, 40), (40, 0), and (40, 40) (unit: cm) and their focus directions were automatically controlled with a step motor. Because the PSA–MPTs have an excellent beam-focusing characteristic, the signal processing for the cracked imaging plate can be relatively simple.

As far as imaging is concerned, omni-directional MPTs can alternatively be used instead of highly directional transducers. In Fig. 19, OL-MPT imaging is shown in the formation of a phased-array system [110]. Among the transducers shown in the figure, four of them were used to form a phased-array transmitting unit and the remaining four MPTs were used as receivers; the excitation frequency was 400 kHz. The advantage of using omni-directional transducers is that various imaging processing algorithms have been developed in related fields such as medical imaging.

Before closing this section, we remark that MPTs can be fabricated in a laboratory, so the production of magnetostrictive transducers can be tailored for use in new experiments. Recent cases include elastic wave experiments for phononic crystals [89–91] and metamaterials [111,112]. Fig. 20(a) shows a giant MPT that was designed to transmit a 180 kHz plane SH wave, with a beam width of 150 mm, for the purpose of experiments in a phononic crystal plate regarding one-sided elastic wave transmission [91]. In Fig. 20(b), the experimental setup for far-field subwavelength imaging experiments which use the 100 kHz ultrasonic S0 Lamb wave in a 2 mm aluminum metamaterial plate is shown in [111]; for the experiment, two sources lying within half the wavelength of the excited Lamb wave should become sufficiently excited to perform imaging beyond the sub-diffraction limit. Specifically,

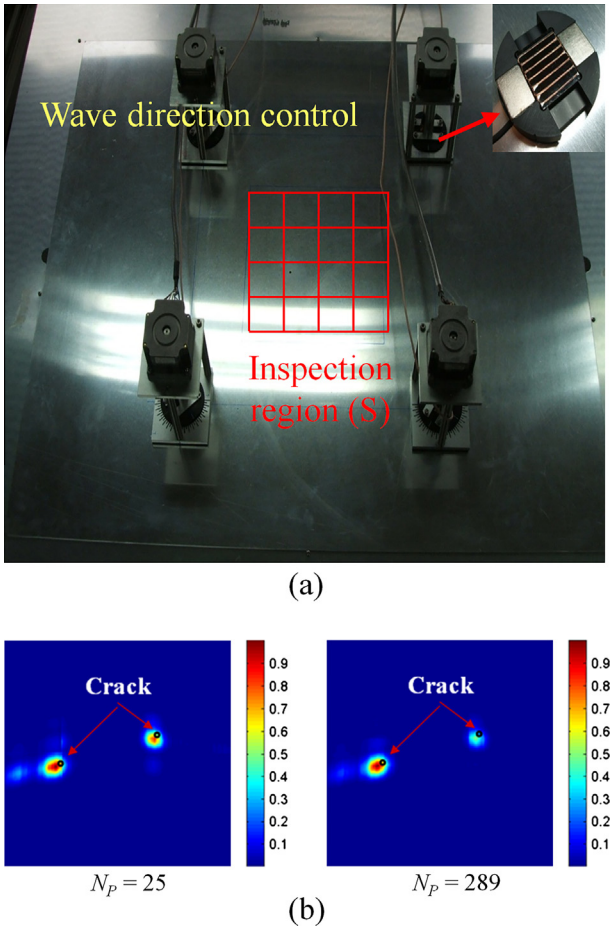

Fig. 18. (a) Photo of the experimental setup for plate imaging by planar solenoid array–magnetostrictive patch transducer (PSA–MPT). (b) Imaging results in a plate having two artificial cracks. The symbol N_p indicates the number of targeting points of the PSA–MPT. (From [89]; reprinted by permission of the American Institute of Aeronautics and Astronautics, Inc.)

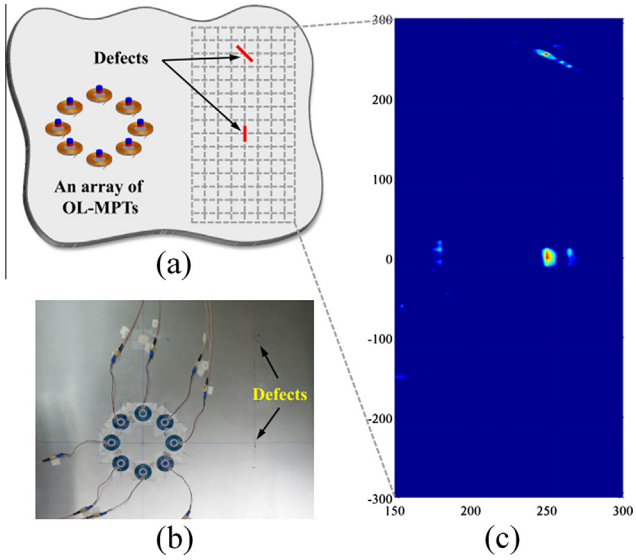

Fig. 19. (From [111]) (a) Illustration of the imaging experimental setup using OL-MPT. (b) Photo of OL-MPT installed on a plate having two artificial cracks. (c) Imaging result.

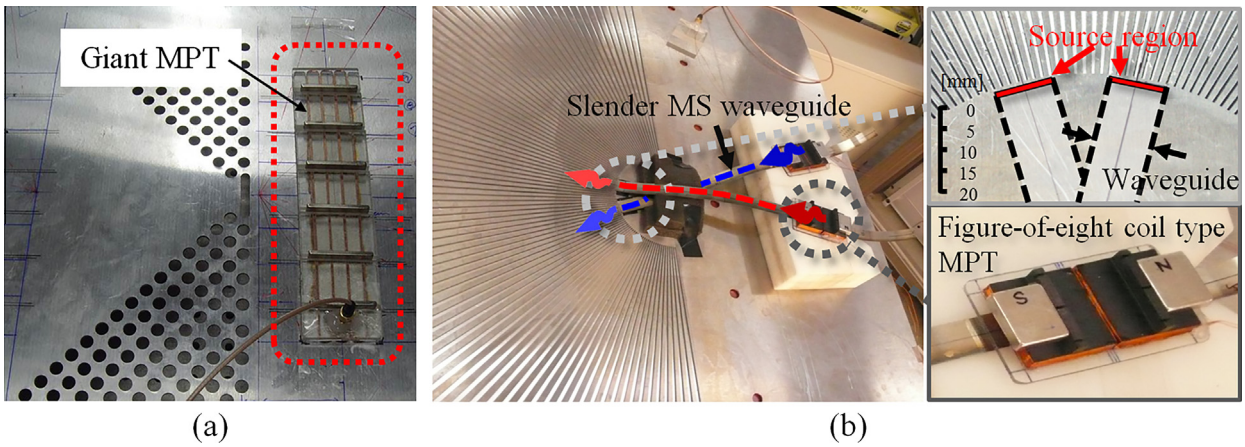

Fig. 20. (a) A giant magnetostrictive patch transducer (MPT) designed to transmit a 180 kHz plane SH wave of 150 mm beam width for one-sided elastic wave transmission experiments in a phononic crystal plate [92]. (b) Experimental setup for a far-field subwavelength imaging experiment using 100 kHz ultrasonic S0 Lamb waves to perform imaging beyond the sub-diffraction limit. (Reprinted with permission from [112]. Copyright 2006, AIP Publishing LLC.)

the center-to-center separation distance between the two sources was 2.47 cm, within which the installation of two wave-source-producing standard transducers was difficult. (This distance is smaller than half the wavelength of the S0 wave at 100 kHz.) The transducer shown in the right-hand figure of Fig. 20(b) was therefore tailor-made, whereby slender magnetostrictive waveguides of a 1.3 cm width and 0.15 mm thickness were prepared, followed by the placement of permanent magnets and a figure-of-eight coil (as used in the MPT of Fig. 4(a)) over the waveguides to generate the desired ultrasonic waves.

5. Conclusions

Through a review of various magnetostrictive patch transducers, this paper argued that an understanding of the operational magnetostrictive phenomena is important for the design of MPTs: the Joule and Villari effects represent interactions between the magnetic field and normal strain (stress), and the Wiedemann and reverse Wiedemann effects represent interactions between the magnetic field and shear strain (stress). To develop transducers that require linear input–output behavior, a static bias magnetic field is necessary and the magnitude of an applied magnetic field should be considerably smaller than the bias field; therefore, three key components of MPTs are magnetostrictive patches, coils for dynamic-field supply, and magnets for static-field supply. (Static field can be also supplied by means other than magnets.) As dynamic mechanical deformations in magnetostrictive patches generate elastic waves in waveguides, an understanding of dispersion characteristics in waveguides is essential for those seeking to design an MPT.

MPTs in cylindrical waveguides such as pipes and cylinders can actually generate any type of wave mode, but the use of MPTs may be most attractive for generating high-power torsional wave modes which would be difficult or cost-ineffective with other transducers; for this reason, the MPTs for torsional waves were mainly discussed. Because torsional waves involve shearing strain, it appears natural to use the Wiedemann effect for their generation. Torsional waves at frequencies ranging from a few kilohertz to a megahertz can be successfully generated by using MPTs, but the generation of high-frequency waves at megahertz frequencies is still challenging even if meander coils tuned to the wavelength of a desired wave mode are used. Transducer configurations that can generate and measure torsional waves by using the Joule and Villari effects were also reviewed because they can be installed in rotating shafts. It was also possible to measure low-frequency torsional vibrations of around a few hundred hertz in the propeller shaft of an automobile.

In terms of plate-specific MPTs, both omni-directional and directional MPTs that use circular magnetostrictive patches were reviewed. Regarding the omni-directional Lamb-wave MPT, however, our results cover only the lowest symmetric (S0) wave mode; therefore, further investigation of a method or new MPT that can generate and measure non-symmetric and/or higher wave modes selectively may be warranted. The omni-directional SH-wave MPT operated by the Wiedemann effect was also reviewed. The transducer uses a unique configuration requiring a toroidal coil to be wound over the annular magnetostrictive patch. A special coil-winding technique was needed to provide a uniform magnetic field in the patch. On the other hand, unidirectional Lamb and SH waves of very narrow beam widths can also be generated if planar-solenoid arrays are used to generate dynamic magnetic field in MPTs. In most plate-specific MPTs, circular patches were used. The main reason is that compared with other shapes, circular patch shapes facilitate easy adjustments of the magnetic field directions even with the single installation of a patch onto a plate. The magnetic circuit placed over the patch can be easily and freely rotated to change the beam-focused direction of the generated wave mode; that is, a different wave mode can be excited and measured under a single transducer installation and its propagation direction can be arbitrarily selected. Nevertheless, patches in other shapes including patches with some inhomogeneity may be investigated to improve MPT performance and to expand MPT applications.

MPTs have several advantages such as good sensitivity, durability, no direct wiring to a transducer or a test specimen itself, long-range inspection, easy implementation, and cost-effectiveness; but, they also have some drawbacks. Although MPTs can be used for wave transduction in ferromagnetic waveguides, it is difficult to concentrate magnetic fields of sufficient strength mainly on the magnetostrictive patches of MPTs. Another major difficulty to be overcome appears in high-frequency (over 1 MHz) wave transduction. Because coils (especially solenoids) have high impedances ah high frequencies, the transduction efficiency of MPTs can be poor at higher frequencies. If meander coils are used for megahertz frequency transductions by MPTs (see Fig. 3(a)), multiple lines should be used. In this case, the support of a generated wave in the time domain can be quite long (see Fig. 8(b)) so that signal analysis can be difficult. Internal wave reflection or ringing within a magnetostrictive patch can be also an issue in high-frequency transduction.

Despite the MPT-related drawbacks mentioned above, a critical advantage that MPTs hold over other transducers such as piezoelectric transducers is that MPTs are easily tailor-made for specific goals, which has been demonstrated through experiments in the new research areas of elastic metamaterials and phononic crystals. Furthermore, MPTs are cost-effective and the capability to generate high-powered shear- or torsional-wave modes is very useful. Considering the growing interest in using and designing MPTs that has recently surfaced, the availability of more powerful and versatile MPTs is expected in the near future.

Acknowledgments

This research was supported by the National Research Foundation of Korea (NRF), funded by the Ministry of Science, ICT & Future Planning, Korea (Grant Nos. 2015-021967, 2014-048162 and 2014M3A6B3063711) contracted through the Institute of Advanced Machines and Design at Seoul National University. We thank Joo Kyung Lee, Hong Min Seung, Heung Son Lee, and Joo Hwan Oh for their help in preparing the manuscript. Also discussions with Dr. Seung Hyun Cho at Korea Research Institute of Standards and Science are appreciated.

Appendix A. Details of experiments with MPTs

In Appendix, we will present the detailed setting for an experiment with an MPT in a pipe, depicted in Fig. 8(a). Other kinds of experiments with different MPTs in pipes or plates may be similarly performed.

Fig. 8(a) shows the setup [57] for 1 MHz, torsional-wave-based pitch–catch NDT experiments performed in a cracked aluminum pipe of a 25 mm mean diameter and 2 mm thickness. The configuration of the transducer used for this experiment is shown in Fig. 3(a). The transducer consists of a strip-type magnetostrictive patch that was wound around the circumference of the test pipe, two permanent magnets located in the opposite circumferential direction on the surface of the pipe (their polarities are shown in Fig. 3(a)), and meander coils with a distance of 1.55 mm between each finger. The distance is tuned to excite the lowest torsional wave mode in the pipe. The patch of a 19 mm width and 0.15 mm thickness is made of iron–cobalt alloy (Hiperco 50HS, Carpenter Technology Corp., Wyomissing, PA). Nickel was also used to make a magnetostrictive transducer. The size of each neodymium magnet is 25 mm × 3 mm × 3 mm.

For the experiment, a modulated Gaussian pulse or Gabor function $f_{Gp}(t)$ was employed (e.g., [113] for NDT applications):

$$f_{Gp}(t) = \frac{1}{(\pi\tilde{\sigma})^{\frac{1}{4}}} e^{-\frac{t^2}{2\tilde{\sigma}^2}} \cos \eta t, \tag{17}$$

where η is the center frequency and the parameter $\tilde{\sigma}$ controls the spread of the pulse in time. The Gabor-pulse signal input that was sent to the transmitting MPT was generated by a function generator (33250A by Agilent Technologies) and amplified by a power amplifier (RAM-5000 by Ritec Inc.) The typical peak-to-peak value of an input current to the transmitter after amplification is around a few amperes. The wave signal measured at the receiving MPT was amplified by a low-noise preamplifier (SR 560 by Stanford Research Systems (Sunnyvale, CA)) and sent to a digital oscilloscope (LT-354M, LeCroy). The typical gain for pre-amplification is in the region of 200–500. To remove white noise, the measured signals were averaged over the range of 20–200 samples in the case of torsional experiments.

References

[1] E. Du Trémolet de Lacheisserie, Magnetostriction, CRC Press, 1993.
[2] D.C. Jiles, Theory of the magnetomechanical effect, J. Phys. D: Appl. Phys. 28 (1995) 1537–1546.
[3] J.P. Joule, XVII. On the effects of magnetism upon the dimensions of iron and steel bars, Philos. Mag. Ser. 3 30 (1847) 76–87.
[4] E. Villari, Ueber die aenderungen des magnetischen moments, welche der zug und das hindurchleiten eines galvanischen stroms in einem stabe von stahl oder eisen hervorbringen, Ann. Phys. 202 (1865) 87–122.
[5] G. Wiedemann, Magnetische Untersuchungen, Ann. Phys. 193 (1862) 193–217.
[6] N.S. Tzannes, Joule and Wiedemann effects – the simultaneous generation of longitudinal and torsional stress pulses in magnetostrictive materials, IEEE Trans. Sonics Ultrason. 13 (1966) 33–41.
[7] A. Rothbart, L. Rosenberg, A theory of pulse transmission along a magnetostrictive delay line, IRE Trans. Ultrason. Eng. 5 (1957) 32–58.
[8] R.C. William, Theory of magnetostrictive delay lines for pulse and continuous wave transmission, IRE Trans. Ultrason. Eng. 6 (1959) 16–32.
[9] E. Hristoforou, Magnetostrictive delay lines: engineering theory and sensing applications, Meas. Sci. Technol. 14 (2003) R15–R47.
[10] F.T. Calkins, A.B. Flatau, M.J. Dapino, Overview of magnetostrictive sensor technology, J. Intell. Mater. Syst. Struct. 18 (2007) 1057–1066.
[11] A.E. Clark, J.P. Teter, O.D. McMasters, Magnetostriction "jumps" in twinned Tb0.3Dy0.7Fe1.9, J. Appl. Phys. 63 (1988) 3910–3912.
[12] M. Anjanappa, J. Bi, A theoretical and experimental study of magnetostrictive mini-actuators, Smart Mater. Struct. 3 (1994) 83–91.
[13] M. Anjanappa, Y. Wu, Magnetostrictive particulate actuators: configuration, modeling and characterization, Smart Mater. Struct. 6 (1997) 393–402.
[14] F. Claeyssen, N. Lhermet, R. Le Letty, P. Bouchilloux, Actuators, transducers and motors based on giant magnetostrictive materials, J. Alloys Compd. 258 (1997) 61–73.
[15] Y. Kim, Y.Y. Kim, A novel Terfenol-D transducer for guided-wave inspection of a rotating shaft, Sens. Actuators, A 133 (2007) 447–456.
[16] M.B. Moffett, A.E. Clark, M. Wun-Fogle, J. Linberg, J.P. Teter, E.A. McLaughlin, Characterization of Terfenol-D for magnetostrictive transducers, J. Acoust. Soc. Am. 89 (1991) 1448–1455.
[17] K.S. Kannan, A. Dasgupta, A nonlinear Galerkin finite-element theory for modeling magnetostrictive smart structures, Smart Mater. Struct. 6 (1997) 341–350.
[18] M.J. Dapino, R.C. Smith, L.E. Faidley, A.B. Flatau, A coupled structural-magnetic strain and stress model for magnetostrictive transducers, J. Intell. Mater. Syst. Struct. 11 (2000) 135–152.
[19] J. Kim, E. Jung, Finite element analysis for acoustic characteristics of a magnetostrictive transducer, Smart Mater. Struct. 14 (2005) 1273–1280.
[20] X.J. Zheng, X.E. Liu, A nonlinear constitutive model for Terfenol-D rods, J. Appl. Phys. 97 (2005) 053901.
[21] S. Valadkhan, K. Morris, A. Khajepour, Review and comparison of hysteresis models for magnetostrictive materials, J. Intell. Mater. Syst. Struct. 20 (2009) 131–142.
[22] R.B. Thompson, Mechanisms of electromagnetic generation and detection of ultrasonic Lamb waves in iron–nickel alloy polycrystals, J. Appl. Phys. 48 (1977) 4942–4950.
[23] R.B. Thompson, Generation of horizontally polarized shear waves in ferromagnetic materials using magnetostrictively coupled meander-coil electromagnetic transducers, Appl. Phys. Lett. 34 (1979) 175–177.
[24] H. Kwun, S.Y. Kim, J.F. Crane, Method and apparatus generating and detecting torsional wave inspection of pipes or tubes, U.S. Patent No. 6429650, 6 Aug. 2002.
[25] H. Kwun, C.M. Teller, Magnetostrictive generation and detection of longitudinal, torsional, and flexural waves in a steel rod, J. Acoust. Soc. Am. 96 (1994) 1202–1204.
[26] H. Kwun, S.Y. Kim, G.M. Light, The magnetostrictive sensor technology for long range guided wave testing and monitoring of structures, Mater. Eval. 61 (2003) 80–84.
[27] H. Kwun, M.T.I. Cecil, Nondestructive evaluation of ferromagnetic cables and ropes using magnetostrictively induced acoustic/ultrasonic waves and magnetostrictively detected acoustic emissions, U.S. Patent No. 5456113, 10 Oct. 1995.
[28] H. Kwun, M.T.I. Cecil, Nondestructive evaluation of non-ferromagnetic materials using magnetostrictively induced acoustic/ultrasonic waves and magnetostrictively detected acoustic emissions, U.S. Patent No. 5457994, 17 Oct. 1995.
[29] H. Kwun, K.A. Bartels, Experimental observation of elastic-wave dispersion in bounded solids of various configurations, J. Acoust. Soc. Am. 99 (1996) 962–968.
[30] H. Kwun, K.A. Bartels, C. Dynes, Dispersion of longitudinal waves propagating in liquid-filled cylindrical shells, J. Acoust. Soc. Am. 105 (1999) 2601–2611.
[31] H. Kwun, S.Y. Kim, M.S. Choi, S.M. Walker, Torsional guided-wave attenuation in coal-tar-enamel-coated, buried piping, NDT and E Int. 37 (2004) 663–665.
[32] H. Kwun, J.J. Hanley, A.E. Holt, Detection of corrosion in pipe using the magnetostrictive sensor technique, in: Proc. SPIE 2459, Nondestructive Evaluation of Aging Maritime Applications, 1995, pp. 140–148.

[33] H. Kwun, A.E. Holt, Feasibility of under-lagging corrosion detection in steel pipe using the magnetostrictive sensor technique, NDT and E Int. 28 (1995) 211–214.
[34] H. Kwun, K.A. Bartels, Magnetostrictive sensor technology and its applications, Ultrasonics 36 (1998) 171–178.
[35] H. Kwun, S.Y. Kim, M.S. Choi, Experimental study of shear horizontal wave transmission and reflection at a tee joint, J. Korean Phys. Soc. 44 (2004) 461–463.
[36] H. Kwun, C.M. Teller, Detection of fractured wires in steel cables using magnetorestrictive sensors, Mater. Eval. 52 (1994) 503–507.
[37] Z. Liu, J. Zhao, B. Wu, Y. Zhang, C. He, Configuration optimization of magnetostrictive transducers for longitudinal guided wave inspection in seven-wire steel strands, NDT and E Int. 43 (2010) 484–492.
[38] P.W. Tse, X.C. Liu, Z.H. Liu, B. Wu, C.F. He, X.J. Wang, An innovative design for using flexible printed coils for magnetostrictive-based longitudinal guided wave sensors in steel strand inspection, Smart Mater. Struct. 20 (2011) 055001.
[39] H. Kwun, C.M. Teller, R.C. Meyer, K.R. Swenson, Apparatus and method for monitoring engine conditions, using magnetostrictive sensors, U.S. Patent No. 6212944, 10 Apr. 2001.
[40] R. Murayama, Study of driving mechanism on electromagnetic acoustic transducer for Lamb wave using magnetostrictive effect and application in drawability evaluation of thin steel sheets, Ultrasonics 37 (1999) 31–38.
[41] L. Laguerre, J.-C. Aime, M. Brissaud, Magnetostrictive pulse-echo device for non-destructive evaluation of cylindrical steel materials using longitudinal guided waves, Ultrasonics 39 (2002) 503–514.
[42] H. Lee, Y.Y. Kim, Wave selection using a magnetomechanical sensor in a solid cylinder, J. Acoust. Soc. Am. 112 (2002) 953–960.
[43] H. Kwun, J.F. Crane, S.Y. Kim, A.J. Parvin, G.M. Light, A torsional mode guided wave probe for long range, in bore testing of heat exchanger tubing, Mater. Eval. 63 (2005) 430–433.
[44] H.C. Lee, Mode-selective ultrasonic wave sensor and its characteristics, J. Mech. Sci. Technol. 22 (2008) 247–254.
[45] P. Sun, X. Wu, J. Xu, J. Li, Enhancement of the excitation efficiency of the non-contact magnetostrictive sensor for pipe inspection by adjusting the alternating magnetic field axial length, Sensors 14 (2014) 1544–1563.
[46] M.J. Sablik, S.W. Rubin, Modeling magnetostrictive generation of elastic waves in steel pipes, I. Theory, Int. J. Appl. Electromagn. Mech. 10 (1999) 143–166.
[47] M.J. Sablik, S.W. Rubin, Modeling magnetostrictive generation of elastic waves in steel pipes, II. Comparison to experiment, Int. J. Appl. Electromagn. Mech. 10 (1999) 167–176.
[48] S.H. Cho, Y. Kim, Y.Y. Kim, The optimal design and experimental verification of the bias magnet configuration of a magnetostrictive sensor for bending wave measurement, Sens. Actuators, A 107 (2003) 225–232.
[49] Y.Y. Kim, S.H. Cho, H.C. Lee, Application of magnetomechanical sensors for modal testing, J. Sound Vib. 268 (2003) 799–808.
[50] S.W. Han, H.C. Lee, Y.Y. Kim, Noncontact damage detection of a rotating shaft using the magnetostrictive effect, J. Nondestr. Eval. 22 (2003) 141–150.
[51] R. Ribichini, F. Cegla, P.B. Nagy, P. Cawley, Study and comparison of different EMAT configurations for SH wave inspection, IEEE Trans. Ultrason. Ferroelectr. Freq. Control 58 (2011) 2571–2581.
[52] Guided Ultrasonics Ltd. <http://www.guided-ultrasonics.com/> (accessed 30.12.14).
[53] Teletest FOCUS+. <www.teletestfocus.com/> (accessed 30.13.14).
[54] R. Ribichini, F. Cegla, P.B. Nagy, P. Cawley, Quantitative modeling of the transduction of electromagnetic acoustic transducers operating on ferromagnetic media, IEEE Trans. Ultrason. Ferroelectr. Freq. Control 57 (2010) 2808–2817.
[55] J.H. Oh, K.H. Sun, Y.Y. Kim, Time-harmonic finite element analysis of guided waves generated by magnetostrictive patch transducers, Smart Mater. Struct. 22 (2013) 085007.
[56] M.-S. Choi, S.-Y. Kim, H. Kwun, An equivalent circuit model of magnetostrictive transducers for guided wave applications, J. Korean Phys. Soc. 47 (2005) 454–462.
[57] S.H. Cho, H.W. Kim, Y. Young Kim, Megahertz-range guided pure torsional wave transduction and experiments using a magnetostrictive transducer, IEEE Trans. Ultrason. Ferroelectr. Freq. Control 57 (2010) 1225–1229.
[58] M.S. Choi, S.J. Kim, Contact SH-guided-wave magnetostrictive transducer, U.S. Patent No. 20120091829, 19 Apr. 2012.
[59] S.A. Vinogradov, Method and system for the generation of torsional guided waves using a ferromagnetic strip sensor, U.S. Patent No. 7573261, 11 Aug. 2009.
[60] Z. Liu, J. Fan, Y. Hu, C. He, B. Wu, Torsional mode magnetostrictive patch transducer array employing a modified planar solenoid array coil for pipe inspection, NDT and E Int. 69 (2015) 9–15.
[61] H.W. Kim, S.H. Cho, Y.Y. Kim, Analysis of internal wave reflection within a magnetostrictive patch transducer for high-frequency guided torsional waves, Ultrasonics 51 (2011) 647–652.
[62] K.S. Kumar, V. Murthy, K. Balasubramaniam, Improvement in the signal strength of magnetostrictive ultrasonic guided wave transducers for pipe inspection using a soft magnetic ribbon-based flux concentrator, Insight-Non-Destructive Test. Condition Monit. 54 (2012) 217–220.
[63] H.W. Kim, Y.E. Kwon, J.K. Lee, Y.Y. Kim, Higher torsional mode suppression in a pipe for enhancing the first torsional mode by using magnetostrictive patch transducers, IEEE Trans. Ultrason. Ferroelectr. Freq. Control 60 (2013) 562–572.
[64] H. Kwun, S.-Y. Kim, Measurement of torsional dynamics of rotating shafts using magnetostrictive sensors, U.S. Patent No. 7131339, 7 Nov. 2006.
[65] H. Kwun, E.C. Laiche, A.J. Parvin, Magnetostrictive sensor probe for guided-wave inspection and monitoring of wire ropes/cables and anchor rods, U.S. Patent No. 8098065, 17 Jan. 2012.
[66] H. Kwun, S.Y. Kim, G.M. Light, Improving guided wave testing of pipelines with mechanical attachments, Mater. Eval. 68 (2010) 927–932.
[67] H.W. Kim, H.J. Lee, Y.Y. Kim, Health monitoring of axially-cracked pipes by using helically propagating shear-horizontal waves, NDT and E Int. 46 (2012) 115–121.
[68] T. Hayashi, M. Murase, Defect imaging with guided waves in a pipe, J. Acoust. Soc. Am. 117 (2005) 2134–2140.
[69] H. Kwun, S.-Y. Kim, M.-S. Choi, Reflection of the fundamental torsional wave from a stepwise thickness change in a pipe, J. Korean Phys. Soc. 46 (2005) 1352–1357.
[70] S. Vinogradov, C. Barrera, Development of guided wave examinations of piping and tubing using magnetostrictive sensor technology, in: Proceedings of 8th International Conference on NDE in Relation to Structural Integrity for Nuclear and Pressurized Components, Berlin, Germany, Sep. 29-Oct. 1, 2010.
[71] H.W. Kim, Y.E. Kwon, S.H. Cho, Y.Y. Kim, Shear-horizontal wave-based pipe damage inspection by arrays of segmented magnetostrictive patches, IEEE Trans. Ultrason. Ferroelectr. Freq. Control 58 (2011) 2689–2698.
[72] H.W. Kim, J.K. Lee, Y.Y. Kim, Circumferential phased array of shear-horizontal wave magnetostrictive patch transducers for pipe inspection, Ultrasonics 53 (2013) 423–431.
[73] J.K. Van Velsor, R.L. Royer, S.E. Owens, J.L. Rose, A magnetostrictive phased array system for guided wave testing and structural health monitoring of pipe, Mater. Eval. 71 (2013) 1296–1301.
[74] S.H. Cho, S.W. Han, C.I. Park, Y.Y. Kim, Noncontact torsional wave transduction in a rotating shaft using oblique magnetostrictive strips, J. Appl. Phys. 100 (2006) 104903.
[75] Y.Y. Kim, C.I. Park, S.H. Cho, S.W. Han, Torsional wave experiments with a new magnetostrictive transducer configuration, J. Acoust. Soc. Am. 117 (2005) 3459–3468.
[76] C.I. Park, W. Kim, S.H. Cho, Y.Y. Kim, Surface-detached V-shaped yoke of obliquely bonded magnetostrictive strips for high transduction of ultrasonic torsional waves, Appl. Phys. Lett. 87 (2005) 224105.
[77] C.I. Park, S.H. Cho, Y.Y. Kim, Z-shaped magnetostrictive patch for efficient transduction of a torsional wave mode in a cylindrical waveguide, Appl. Phys. Lett. 89 (2006) 174103.
[78] E. Kannan, B. Maxfield, K. Balasubramaniam, SHM of pipes using torsional waves generated by in situ magnetostrictive tapes, Smart Mater. Struct. 16 (2007) 2505–2515.
[79] H. Kwun, S.-Y. Kim, G.M. Light, Long-range guided wave inspection of structures using the magnetostrictive sensor, J. Korean Soc. NDT 21 (2001) 383–390.
[80] G.M. Light, H. Kwun, S. Kim, R.L. Spinks, Magnetostrictive sensor for active health monitoring in structures, in: Proc. SPIE 4702, Smart Nondestructive Evaluation for Health Monitoring of Structural and Biological Systems, 282 (June 11, 2002).
[81] S.H. Cho, J.S. Lee, Y.Y. Kim, Guided wave transduction experiment using a circular magnetostrictive patch and a figure-of-eight coil in nonferromagnetic plates, Appl. Phys. Lett. 88 (2006) 224101.
[82] J.S. Lee, S.H. Cho, Y.Y. Kim, Radiation pattern of Lamb waves generated by a circular magnetostrictive patch transducer, Appl. Phys. Lett. 90 (2007) 054102.
[83] J.S. Lee, Y.Y. Kim, S.H. Cho, Beam-focused shear-horizontal wave generation in a plate by a circular magnetostrictive patch transducer employing a planar solenoid array, Smart Mater. Struct. 18 (2009) 015009.
[84] L. Zhou, Y. Yang, F.-G. Yuan, Design of a magnetostrictive sensor for structural health monitoring of non-ferromagnetic plates, J. Vibroeng. 14 (2012) 280–291.
[85] B. Yoo, S.-M. Na, A.B. Flatau, D.J. Pines, Directional magnetostrictive patch transducer based on Galfenol's anisotropic magnetostriction feature, Smart Mater. Struct. 23 (2014) 095035.
[86] J.K. Lee, H.W. Kim, Y.Y. Kim, Omnidirectional Lamb waves by axisymmetrically-configured magnetostrictive patch transducer, IEEE Trans. Ultrason. Ferroelectr. Freq. Control 60 (2013) 1928–1934.
[87] H.M. Seung, H.W. Kim, Y.Y. Kim, Development of an omni-directional shear-horizontal wave magnetostrictive patch transducer for plates, Ultrasonics 53 (2013) 1304–1308.
[88] J.S. Lee, H.W. Kim, B.C. Jeon, S.H. Cho, Y.Y. Kim, Damage detection in a plate using beam-focused shear-horizontal wave magnetostrictive patch transducers, AIAA J. 48 (2010) 654–663.
[89] M.K. Lee, P.S. Ma, I.K. Lee, H.W. Kim, Y.Y. Kim, Negative refraction experiments with guided shear-horizontal waves in thin phononic crystal plates, Appl. Phys. Lett. 98 (2011) 011909.
[90] P.S. Ma, H.W. Kim, J.H. Oh, Y.Y. Kim, Mode separation of a single-frequency bi-modal elastic wave pulse by a phononic crystal, Appl. Phys. Lett. 99 (2011) 201906.
[91] J.H. Oh, H.W. Kim, P.S. Ma, H.M. Seung, Y.Y. Kim, Inverted bi-prism phononic crystals for one-sided elastic wave transmission applications, Appl. Phys. Lett. 100 (2012) 213503.

[92] S.H. Cho, B.Y. Ahn, T.H. Heo, Magnetostrictive phased array transducer for transducing shear horizontal bulk waves, U.S. Patent No. 20130145851, 13 Jun. 2013.
[93] Y.E. Kwon, H.J. Jeon, H.W. Kim, Y.Y. Kim, Waveguide tapering for beam-width control in a waveguide transducer, Ultrasonics 54 (2014) 953–960.
[94] C. Liang, B. Prorok, Measuring the thin film elastic modulus with a magnetostrictive sensor, J. Micromech. Microeng. 17 (2007) 709–716.
[95] A.V. Krishnamurthy, M. Anjanappa, Z. Wang, X. Chen, Sensing of delaminations in composite laminates using embedded magnetostrictive particle layers, J. Intell. Mater. Syst. Struct. 10 (1999) 825–835.
[96] E. Saidha, G.N. Naik, S. Gopalkrishnan, An experimental investigation of a smart laminated composite beam with a magnetostrictive patch for health monitoring applications, Struct. Health Monit. 2 (2003) 273–292.
[97] D.P. Ghosh, S. Gopalakrishnan, Coupled analysis of composite laminate with embedded magnetostrictive patches, Smart Mater. Struct. 14 (2005) 1462–1473.
[98] K.F. Graff, Wave Motion in Elastic Solids, Courier Dover Publications, 1975.
[99] J.L. Rose, Ultrasonic Waves in Solid Media, Cambridge University Press, 2004.
[100] D.C. Gazis, Three-dimensional investigation of the propagation of waves in hollow circular cylinders. I. Analytical Foundation, J. Acoust. Soc. Am. 31 (1959) 568–573.
[101] G. Engdahl, Handbook of Giant Magnetostrictive Materials, Academic Press, 2000.
[102] M. Hirao, H. Ogi, EMATs for Science and Industry: Noncontacting Ultrasonic Measurements, Springer, 2003.
[103] K.H. Sun, S.H. Cho, Y.Y. Kim, Topology design optimization of a magnetostrictive patch for maximizing elastic wave transduction in waveguides, IEEE Trans. Magn. 44 (2008) 2373–2380.
[104] H.J. Kim, J.S. Lee, H.W. Kim, H.S. Lee, Y.Y. Kim, Numerical simulation of guided waves using equivalent source model of magnetostrictive patch transducers, Smart Mater. Struct. 24 (2015) 015006.
[105] Y.-G. Kim, H.-S. Moon, K.-J. Park, J.-K. Lee, Generating and detecting torsional guided waves using magnetostrictive sensors of crossed coils, NDT and E Int. 44 (2011) 145–151.
[106] S.H. Cho, S.W. Han, C.I. Park, Y.Y. Kim, High-frequency torsional modal testing of a long cylinder by magnetostriction, Appl. Phys. Lett. 91 (2007) 071908.
[107] S.H. Cho, H.S. Kwon, B.Y. Ahn, S.S. Lee, Method and apparatus for monitoring wall thinning of a pipe using magnetostrictive transducers and variation of dispersion characteristics of broadband multimode shear horizontal (SH) waves, U.S. Patent No. 8432159, 30 Apr. 2013.
[108] S.H. Cho, C.I. Park, Y.Y. Kim, Effects of the orientation of magnetostrictive nickel strip on torsional wave transduction efficiency of cylindrical waveguides, Appl. Phys. Lett. 86 (2005) 244101.
[109] Y.Y. Kim, C.I. Park, S. H. Lee, Torsional vibration experiment of a propeller shaft of a rear wheel drive van, IDEALAB Report No. 2008–01 (unpublished) (2008).
[110] J.K. Lee, Y.E. Kwon, H.S. Lee, H.M. Seung, K.Y. Kim, J.K. Lee, H.W. Kim, H.C. Lee, Y.Y. Kim, Development and application of phased array system for defect imaging in plate-like structures, Trans. KSNVE 24 (2014) 123–130.
[111] H.J. Lee, H.W. Kim, Y.Y. Kim, Far-field subwavelength imaging for ultrasonic elastic waves in a plate using an elastic hyperlens, Appl. Phys. Lett. 98 (2011) 241912.
[112] J.H. Oh, H.M. Seung, Y.Y. Kim, A truly hyperbolic elastic metamaterial lens, Appl. Phys. Lett. 104 (2014) 073503.
[113] J.-C. Hong, K.H. Sun, Y.Y. Kim, The matching pursuit approach based on the modulated Gaussian pulse for efficient guided-wave damage inspection, Smart Mater. Struct. 14 (2005) 548–560.